EES Batteries

REVIEW

View Article Online
View Journal

Cite this: DOI: 10.1039/d5eb00244c

Band alignment and interfacial electrostatics: unraveling the dynamic space charge layer in all-solid-state batteries

Haoyuan Lai,[a,b] Jinli Liu,[c] Qiqiang Huang,[a,b] Chenxi Li,[a] Peng Zhang,[a] Xiaofeng Luo,[a] Lewei Shi,[a] Zhibo Han,[a] Wei Peng,[a] Xingtai Liu,[a] Xinman Chen,[b] Languang Lu,[c] Xuning Feng,[c] Dongsheng Ren,[c] Minggao Ouyang *[c] and Xiang Liu *[a]

All-solid-state batteries (ASSBs) are poised to transform electrochemical energy storage, yet their performance remains critically limited by high interfacial impedance. A central origin of this bottleneck is the space charge layer (SCL), an intrinsic electrostatic structure arising from electrochemical potential mismatch at solid–solid interfaces. Unlike the adaptive electric double layers in liquid electrolytes, SCLs in solids form rigid but dynamically evolving potential barriers that vary with state of charge and strongly regulate lithium-ion transport and interfacial stability. This review provides a critical and unified assessment of SCL physics in ASSBs by integrating defect chemistry, semiconductor band theory, and emerging *operando* characterization. We clarify SCL formation driven by Fermi level alignment, reconcile divergent views on its quantitative impact on interfacial resistance, and highlight recent experimental advances that directly visualize buried electrostatic fields. Importantly, we systematically compare two major classes of SCL regulation strategies—hierarchical band alignment engineering and interfacial field modulation—by analyzing their applicable electrolyte systems, processing complexity, scalability, and cost implications. While band alignment engineering *via* buffer or coating layers is particularly effective for oxide-based systems with severe electrostatic mismatch, field modulation strategies offer lower-cost and more scalable solutions for sulfide and composite electrolytes. By explicitly linking interfacial electrostatics to practical material selection and engineering constraints, this review establishes a physically grounded framework for tailoring SCL behavior and provides actionable guidance for the design of next-generation, high-performance ASSBs.

Received 26th December 2025,
Accepted 21st February 2026

DOI: 10.1039/d5eb00244c

rsc.li/EESBatteries

Broader context

All-solid-state batteries (ASSBs) are widely viewed as a cornerstone of next-generation energy storage, offering improved safety and higher energy density compared to conventional liquid-based systems. However, their widespread application is critically limited by interfacial challenges, among which the space charge layer (SCL) plays a central, yet insufficiently understood role. Originating from Fermi level mismatch, the SCL governs lithium-ion redistribution, interfacial electric fields, and kinetic barriers, thus strongly influencing battery performance and degradation. In this work, we establish a comprehensive and multiscale framework to elucidate the formation and evolution of SCLs and their coupling with electrochemical and mechanical effects. By integrating theoretical modeling with advanced characterization techniques, we reveal how SCL-induced changes in activation energy, local current distribution, and ion transport pathways lead to increased impedance and structural instability, particularly under varying states of charge. Importantly, we highlight the dynamic and spatially heterogeneous nature of SCL effects, by bridging microscopic mechanisms with macroscopic performance. These advances provide critical insights into interfacial regulation strategies and offer general design principles for stabilizing solid–solid interfaces, and thereby accelerate the development of high-performance, durable ASSBs and advancing the broader field of electrochemical energy storage.

1. Introduction

Amidst the global energy structure's transition towards decarbonization, high-energy-density lithium-ion batteries have emerged as the primary energy storage solution for electric vehicles and smart grids.[1–7] While current mainstream lithium-ion batteries still rely on liquid electrolytes, these tra-

[a]School of Materials Science and Engineering, Beihang University, 100191 Beijing, China. E-mail: xiangliu@buaa.edu.cn
[b]School of Electronic Science and Engineering (School of Microelectronics) South China Normal University, Foshan 528225, P. R. China
[c]School of Vehicle and Mobility, Tsinghua University, 100084 Beijing, China. E-mail: ouymg@tsinghua.edu.cn

ditional systems exhibit limitations such as low ignition points and poor thermal stability, rendering them susceptible to fire or explosion incidents.[8–10] Furthermore, advancements in technology have pushed the energy density of these batteries close to the theoretical limits of their constituent materials. This is increasingly insufficient to meet the demands for long-range operation and enhanced safety in electric vehicles.[11–13] All-solid-state batteries (ASSBs) are regarded as a cornerstone for next-generation energy storage owing to their intrinsic safety, wide electrochemical stability window, and potential for high-voltage operation. Despite the rapid development of high-conductivity solid electrolytes (10^{-3}–10^{-2} S·cm^{-1}), the interfacial ionic resistance between solid electrolytes and electrodes typically ranges from 10 to 1000 Ω·cm^{-2}, remaining two to four orders of magnitude higher than in liquid systems. This discrepancy constitutes one of the key bottlenecks impeding the practical implementation of ASSBs.[14–19] While earlier studies mainly attributed this resistance to chemical incompatibility and mechanical detachment, such explanations fail to account for persistent interfacial polarization even in chemically stable systems (*e.g.*, $LiNbO_3$-coated $LiCoO_2$/LiPON or oxide–oxide interfaces).[20–26] This observation suggests the presence of an intrinsic electrostatic origin—the space charge layer (SCL)—resulting from the mismatch of Fermi levels, ion chemical potentials, or defect concentrations across the interface. Unlike liquid electrolytes where ions can freely rearrange to screen potentials, the immobile lattice in solid electrolytes facilitates the formation of extended depletion or accumulation zones, fundamentally altering transport kinetics.[1,2,11,12,27,28]

The concept of the SCL in ionic solids has evolved over more than six decades, bridging classical defect chemistry, semiconductor physics, and modern battery science. A concise historical timeline (as shown in Fig. 1) can effectively illustrate this evolution: the idea of a space charge region was first introduced by W. Schottky in the context of semiconductor heterojunctions, where potential discontinuities were shown to redistribute charge carriers near the interface. Similar phenomena were later reported in ionic conductors, where heterointerfaces were found to induce local potential gradients and, in some cases, enhance ionic conductivity.[29]

In the early 21st century, Haruyama *et al.*[31] employed density functional theory (DFT) calculations to demonstrate that inserting a suitable buffer layer could effectively mitigate the lithium-ion depletion or accumulation caused by SCL formation at solid–solid interfaces. This marked the beginning of rational interface design based on electronic structure. Subsequently, the magnitude of the SCL impact became a subject of debate. De Klerk *et al.*[35] used atomistic simulations to estimate the SCL thickness to be less than 1 nm, suggesting that its impact on ionic transport might be negligible under certain conditions. In contrast, Cheng *et al.*[32] experimentally tuned the interfacial electrochemical potential difference *via in situ* NMR measurements and cathode potential control, showing that the presence of an SCL significantly increases the Li^+ migration barrier at the interface.

Recent advancements in characterization have provided deeper insights into the dynamic nature of these layers. Hikima *et al.*[33] applied *in situ* XPS to monitor band structure evolution during cycling, revealing that the direction of band bending reverses at different states of charge. More recently, researchers have recognized that SCLs do not always hinder ion transport; under specific configurations, they can even facilitate interfacial Li^+ conduction. For example, Ohta *et al.*[34] reported that the LiCl/FeOCl heterointerface (LFH composite) exhibits higher ionic conductivity than either single-phase material, highlighting that a moderate interfacial potential offset may create a fast-ion migration pathway. This historical progression underscores that the SCL is not merely a side effect of interface reactions but a fundamental electrostatic phenomenon intrinsic to solid–solid contact in ionic conductors.

In ASSBs, the SCL dictates the local electrostatic potential, defect concentration, and effective ionic/electronic conductivity near interfaces. These changes, though confined within a few nanometers, can dramatically alter the overall cell impedance and electrochemical stability.[36–41] Despite substantial progress, a comprehensive and quantitative understanding of SCLs in ASSBs remains elusive. Previous reviews often focused on chemical or mechanical aspects, leaving the electrostatic and band-structure perspective fragmented.

In this review, we aim to summarize the fundamental theories and experimental evidence of SCL formation in various solid-state battery systems, compare state-of-the-art characterization techniques capable of probing the SCL at atomic to mesoscale resolution, and discuss materials and interface-engineering strategies—such as band-alignment control and dielectric-layer coatings—to mitigate or exploit the SCL. Finally, we highlight emerging opportunities in multi-physics modeling and *operando* probes that could unify chemical, electrical, and mechanical effects at the solid–solid interface.

2. The formation of the SCL

In liquid electrolytes, mobile ions can rapidly rearrange to maintain electroneutrality at the electrode–electrolyte interface. Potential differences are screened within angstrom-scale distances by solvated ions, forming a compact electric double layer (EDL) with negligible internal field. However, in solid electrolytes, both ionic and electronic mobilities are drastically reduced. The redistribution of charged species becomes limited, preventing complete neutralization of interfacial charge imbalance. Consequently, an extended electrostatic potential gradient develops across the solid–solid interface, forming a SCL that cannot be efficiently screened as in liquid systems. This transition—from dynamic solvation equilibrium in liquids to electrostatic equilibrium in solids—marks a fundamental distinction that governs interfacial transport behavior in ASSBs.

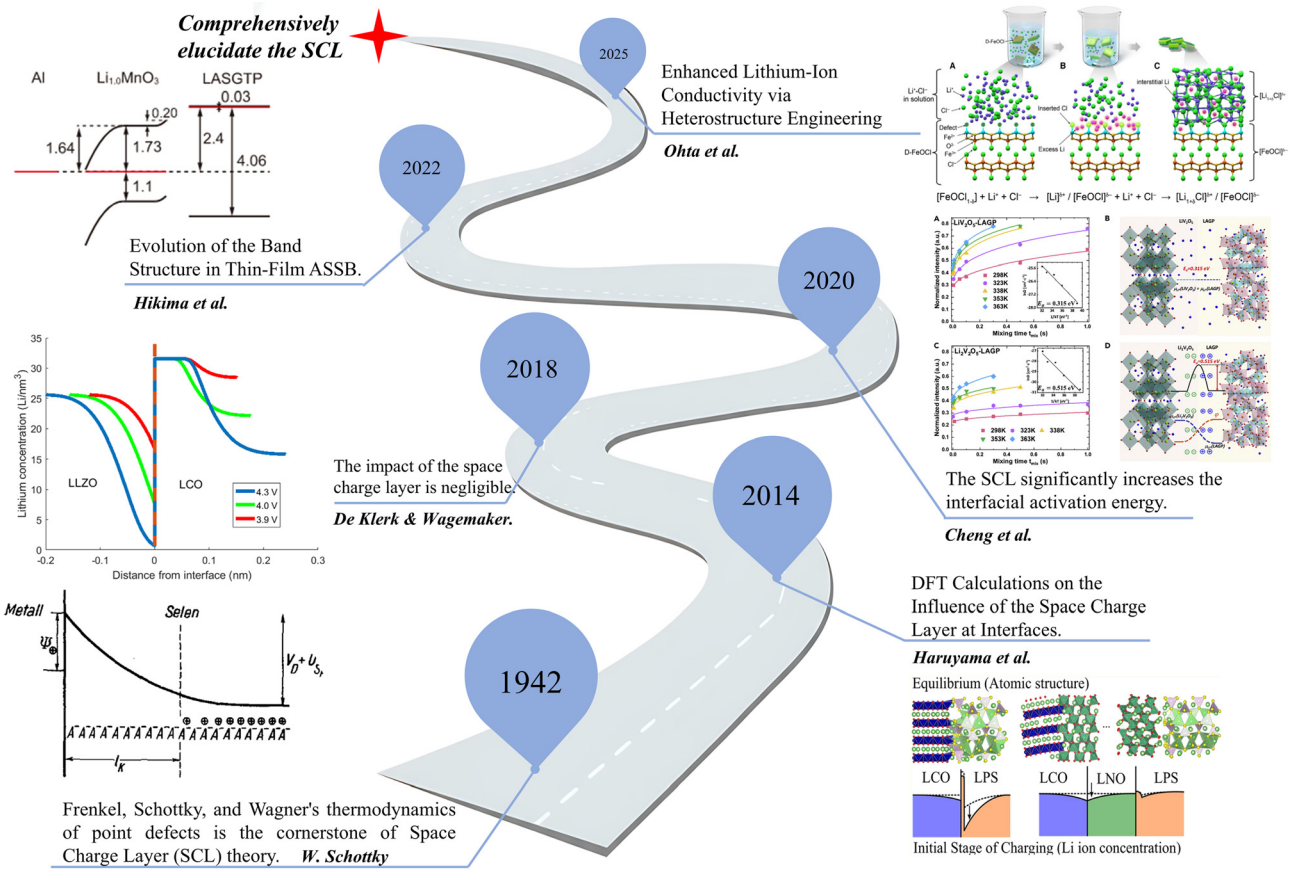

Fig. 1 Historical evolution of the space charge layer concept in solid-state ionics and batteries.[30] Copyright 2004, AIP Publishing. Reproduced with permission.[31] Copyright 2014, American Chemical Society. Reproduced with permission.[32] Copyright 2020, Elsevier. Reproduced under terms of the CC-BY license.[33] Copyright 2022, Kazuhiro Hikima *et al.*, published by Springer Nature. Reproduced with permission.[34] Copyright 2025, Elsevier.

2.1 Origin of the space charge layer

When two solids with different Fermi levels and ionic chemical potentials come into contact, ions and/or electrons migrate across the interface until the electrochemical potential ($\tilde{\mu} = \mu + z{\cdot}e\varphi$) of each species reaches equilibrium. This redistribution disrupts local charge neutrality and produces an electric potential gradient ($d\varphi/dx$) near the interface. The resulting regions of Li^+ enrichment or depletion form the SCL, which modifies local ion concentration and conductivity. The potential profile within the SCL follows Poisson's equation:

$$\frac{d2\phi}{dx^2} = -\frac{\rho(x)}{\varepsilon_0\varepsilon_r}$$

where $\rho(x)$ is the charge density, ε_0 the vacuum permittivity, and ε_r the dielectric constant of the electrolyte. The characteristic length over which the potential decays, known as the Debye length (λ_D), is given by:

$$\lambda_D = \sqrt{\frac{\varepsilon_0\varepsilon_r k_B T}{n_0 q^2}}$$

where k_B is the Boltzmann constant, T is the absolute temperature, n_0 represents the effective concentration of mobile ionic charge carriers participating in electrostatic screening, and q is the elementary charge.

Using representative parameters reported for typical solid electrolytes at room temperature, sulfide electrolytes (*e.g.*, LGPS- or argyrodite-type systems) are commonly characterized by relatively high dielectric constants ($\varepsilon_r \approx 20$–40)[42–45] and high concentrations of mobile Li^+ carriers ($n_0 \approx 10^{21}$ cm^{-3}), reflecting their high ionic conductivity. Substituting these values into the Debye expression yields a characteristic screening length below 1 nm. In contrast, oxide electrolytes such as garnet-type or NASICON-type materials typically exhibit lower dielectric constants ($\varepsilon_r \approx 8$–12)[42–45] and lower effective mobile carrier concentrations ($n_0 \approx 10^{19}$ cm^{-3}), resulting in a Debye length on the order of several nanometers. From a purely electrostatic screening perspective, oxide electrolytes therefore intrinsically support spatially broader SCLs than sulfide electrolytes.[35,46]

However, the electrochemical impact of an SCL is not determined by its spatial extent alone, but by the combined effect of the screening length and the interfacial lithium chemical potential mismatch ($\Delta\mu_{Li}$) between the electrolyte and the electrode. For a given positive electrode material, sulfide electrolytes generally exhibit a larger lithium chemical potential

difference than oxide electrolytes, owing to their higher-lying valence bands and reduced thermodynamic stability at high potentials. The characteristic interfacial electric field can be approximated as:

$$E \sim \frac{\Delta\phi}{\lambda_D} \approx \frac{\Delta\mu_{Li}/e}{\lambda_D}$$

For oxide-based interfaces, $\Delta\mu_{Li}$ is often limited to ~0.1 V, distributed over a Debye length of several nanometers (~2 nm), resulting in electric fields on the order of 10^7 V m^{-1}. In contrast, sulfide-based electrolytes in contact with the same cathode material can experience a larger chemical potential mismatch (~0.3–0.5 V), concentrated within a much shorter screening length (~0.2 nm), giving rise to interfacial electric fields approaching or exceeding 10^8 V m^{-1}. Therefore, although sulfide electrolytes possess a shorter intrinsic Debye length, the combination of a larger lithium chemical potential mismatch and a compressed screening region leads to a stronger and more abrupt interfacial electric field compared to oxide electrolytes. This explains why sulfide-based cathode interfaces often exhibit more pronounced space-charge-driven effects—such as severe lithium depletion or accumulation, enhanced electronic leakage, and accelerated interfacial degradation—even though the nominal SCL thickness is smaller.

This analysis highlights that SCL impact in ASSBs should be evaluated not solely in terms of spatial extent, but through the coupled consideration of electrostatic length scales and chemical potential driving forces.

2.2 The SCL formed at the cathode side of ASSB

The space charge effect is generally more pronounced at the cathode–electrolyte interface than at the anode side for several intrinsic reasons. First, layered oxide cathodes undergo substantial changes in lithium activity during delithiation, leading to a much stronger variation in their electrochemical potential compared with typical anode materials. Second, the potential difference between the cathode and solid electrolyte is intrinsically larger than that between the anode and electrolyte, resulting in a stronger driving force for charge redistribution and more significant band bending at the interface. Third, the cathode operates at much higher potentials, where parasitic reactions and electrolyte decomposition are more likely to occur, creating a chemically complex and dynamically evolving interfacial environment that further amplifies SCL formation.[47] Unlike the subnanometer electric double layer formed in liquid electrolytes, the extended SCL in solid-state systems enables substantial variations in band structure and defect concentration, determined by the electronic character (*e.g.*, n-type or p-type) and defect chemistry of the materials involved.

Goodenough *et al.*[48] demonstrated that the difference in the chemical potential of lithium between the positive and negative electrodes in lithium batteries is primarily dictated by the difference in the electrochemical potential of electrons (*i.e.*, the Fermi level), which governs the open-circuit voltage of the battery. This observation underscores the importance of Fermi level research in battery science. Extending this concept to solid–solid interfaces, mismatched Fermi levels between the cathode and solid electrolyte drive electron and ion redistribution until thermodynamic equilibrium is achieved. This process generates band bending and establishes an internal electric field at the interface. Experimental studies have confirmed that such charge redistribution results in Li^+ enrichment on the electrolyte side for various cathode–electrolyte combinations.[35,49,50]

However, this redistribution can also result in undesirable Li^+-depleted regions ("Li-poor layers"), increased interfacial resistance, and accelerated performance degradation during prolonged cycling. These challenges remain major barriers to achieving high-rate and long-life all-solid-state batteries. Accordingly, interface engineering strategies—particularly the incorporation of electronically insulating buffer layers—have emerged as effective methods to moderate band bending, suppress excessive SCL formation, and stabilize the cathode–electrolyte interface.[29,30,51] Moreover, with the continuous advancement of characterization techniques, we have gradually uncovered some properties of the SCL.

3. The SCL effect

Existing research on the space charge layer is typically categorized into three aspects: first, macroscopic manifestations, such as the increase in interfacial impedance, particularly at the cathode–solid electrolyte interface; second, microscopic characterization, focusing on the enrichment or depletion of lithium-ion or electron concentration at the interface; and third, predictions derived from theoretical calculations or simulation models. However, a definitive consensus on the precise impact of the space charge layer remains elusive. The prevailing view is that the space charge layer contributes to the increase in interfacial impedance. The elucidation of its underlying mechanisms is often confined to specific aspects, and a unified theory comprehensively explaining its impact is still lacking. Given the occasional equivalence of chemical potential and Fermi level under certain conditions, analyzing interface properties through the material's Fermi level offers a valuable perspective. The Fermi level's position dictates the formation and extent of the space charge layer. Ideally, consistent Fermi level alignment across the interface should prevent the generation of a built-in electric field, as depicted in Fig. 2a. With consistent Fermi levels, no chemical potential difference and consequently no band bending would occur. Conversely, Fig. 2b and d illustrate scenarios where the interface Fermi levels are misaligned. This Fermi level mismatch leads to band bending upon interfacial contact, thereby generating a built-in electric field and elevating the interfacial impedance. However, it is crucial to recognize that unlike semiconductor materials, batteries undergo lithium-ion and electron intercalation/deintercalation during charging and discharging. This process induces constant fluctuations in the cathode's Fermi level. Consequently, completely eliminating the space charge layer

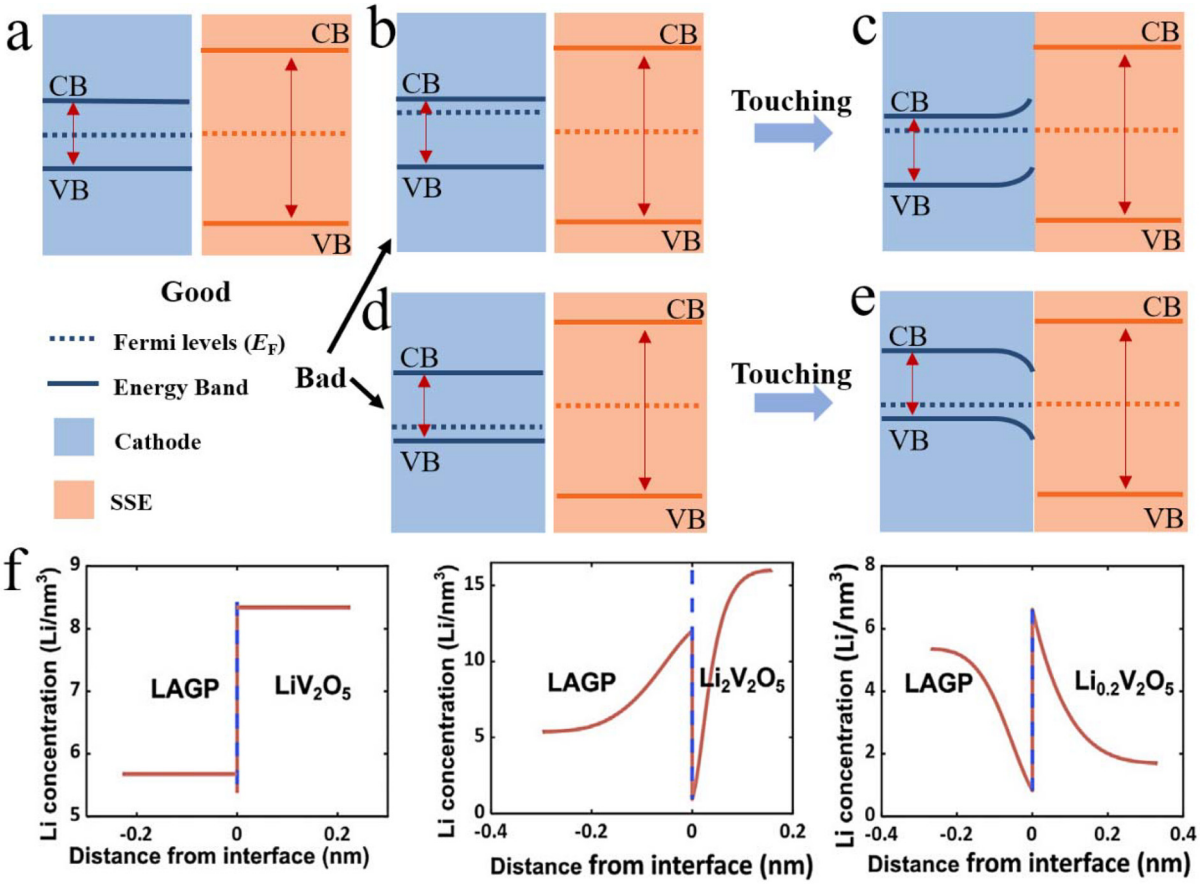

Fig. 2 Schematic diagram of interface Fermi level matching. (a) A good interface state does not lead to band bending at the interface and does not produce a built-in electric field. (b–e) Mismatched Fermi levels, after the unification of Fermi levels, band bending occurs. (f) Lithium-ion aggregation phenomenon caused by different Fermi levels at the interface. Reproduced with permission.[52] Copyright 2020, Elsevier.

based solely on Fermi level matching might not be feasible.[33] Nevertheless, its impact can be mitigated by, for example, identifying materials whose Fermi level shifts are less sensitive to lithium-ion intercalation or deintercalation, thereby alleviating the issues arising from Fermi level disparities. Alternatively, the use of an appropriate buffer layer can mitigate the SCL resulting from an excessive energy level difference.

3.1 Impact of SCL on the interface

The impact of the space charge layer on the interface has been reported by numerous studies. Some researchers posit that the influence of the space charge layer on the interface can be negligible—for example, Haruta *et al.*'s (2015) study utilizing magnetron sputtering to fabricate all-solid-state thin-film batteries found interfacial resistance to be almost negligible.[53] De Klerk and Wagemaker have presented theoretical calculations indicating that the space charge layer at the interface is very thin (less than 1 nanometer) and its impact can be disregarded.[54] However, the majority of the scientific community still maintains that the space charge layer exerts a significant influence on the interface. The main effects attributed to the space charge layer on the interface are generally categorized into three types: alterations and imbalances in lithium-ion concentration; changes in interfacial activation energy; and increases in interfacial impedance. Fig. 3 summarizes the phenomena currently believed to be induced by the space charge layer. These phenomena ultimately manifest as elevated interfacial impedance, leading to a deterioration in the battery's rate and cycle performance.[55–58]

3.1.1 Changes and imbalances in lithium-ion concentration. The presence of the space charge layer can influence the ion concentration at the interface, potentially leading to the depletion of lithium ions and consequently affecting their migration. In 2014, Haruyama *et al.*[31] employed first-principles calculations (DFT) to assess the stability and migration behavior of lithium ions at the interface. They evaluated the susceptibility to SCL formation by calculating the formation energy of lithium vacancies, proposing that the space charge layer can alter the ion concentration at the interface, thereby impacting lithium-ion transport. Conversely, De Klerk and Wagemaker utilized model calculations indicating that the thickness of the space charge layer is typically on the nanoscale, suggesting a relatively minor impact on lithium-ion transport. However,

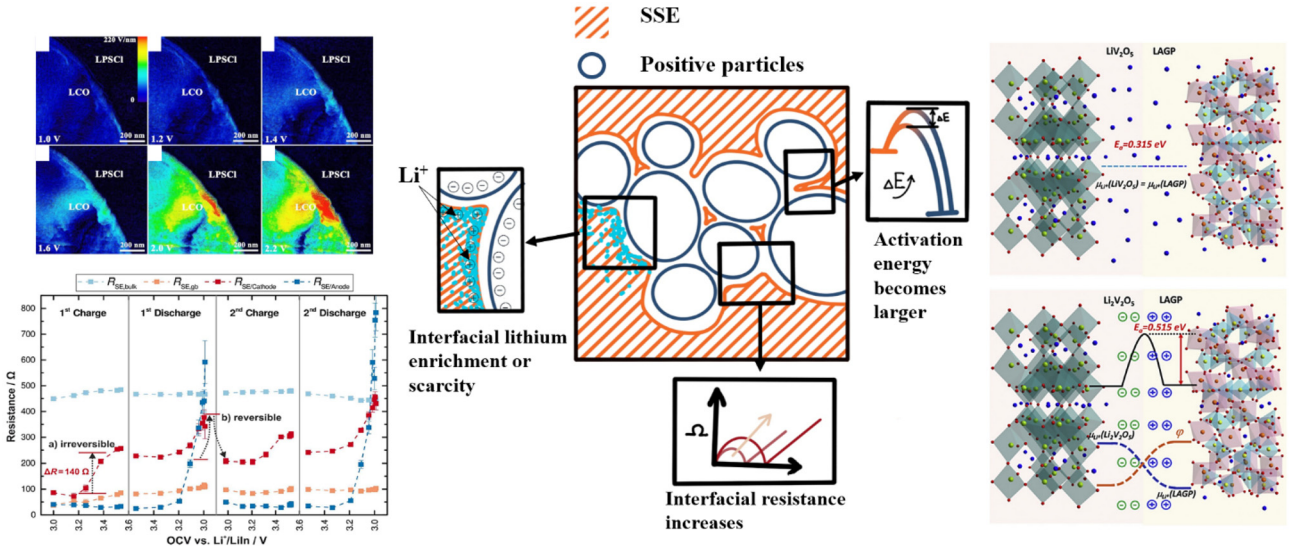

Fig. 3 Impact of the space charge layer on the interface of all-solid-state batteries.

they also acknowledged that in specific scenarios, such as significant lithium-ion depletion, the interfacial resistance caused by the space charge layer may increase substantially.[35] Yamamoto *et al.*[59] employed quantitative electron holography (EH) to directly observe the changes in potential distribution resulting from lithium-ion diffusion in all-solid-state LIBs, revealing the potential distribution of lithium ions at the cathode/solid electrolyte interface during charge–discharge reactions. Yu *et al.*[60] further highlighted that the space charge layer can lead to localized lithium-ion depletion, thereby increasing the energy barrier for lithium-ion transport at the solid electrode–electrolyte interface. In all-solid-state batteries, the potential difference at the interface can further exacerbate the limitation of lithium-ion transport due to the formation of the space charge layer, particularly when the contact area at the interface is limited. These studies collectively demonstrate the significant impact of the space charge layer on the distribution and transport of lithium ions, underscoring that optimizing interface design to mitigate the effects of the space charge layer is crucial for enhancing the performance of all-solid-state batteries (Fig. 4).

3.1.2 Changes in interfacial activation energy. The presence of the space charge layer can elevate the interfacial activation energy barrier, consequently affecting the lithium-ion transport efficiency (Fig. 5). Brogioli *et al.*[63] employed theoretical analysis and experimental validation to elucidate the formation mechanism and impact of the space charge layer at the LLZO/PEO interface. Their findings indicated that the high resistance at this interface primarily originates from the high activation energy, rather than the electrostatic repulsion of lithium ions. By varying the concentration of lithium ions in PEO, they observed changes in interfacial resistance and explained these phenomena using a theoretical model.[63] Cheng *et al.*[32] utilized nuclear magnetic resonance (NMR) two-dimensional exchange experiments to quantitatively study the influence of the space charge layer at the $Li_xV_2O_5$/LAGP interface on lithium-ion transport. Their results showed that the activation energy for lithium-ion exchange was 0.315 eV in the absence of a space charge layer, while it significantly increased to 0.515 eV with the presence of the space charge layer. This indicates that the space charge layer substantially raises the energy barrier for lithium-ion transport. Katzenmeier *et al.* used electrochemical impedance spectroscopy (EIS) to investigate the space charge layer between a model solid-state electrolyte (Ohara LICGC glass) and a gold electrode. They found that the activation energy of the space charge layer was approximately 0.42 eV, higher than the 0.39 eV of the electrolyte bulk.[64,65] Furthermore, they verified that the thickness of the space charge layer is proportional to the square root of the temperature, which aligns with the theoretical prediction of the Debye length. These studies collectively demonstrate that the space charge layer has a notable impact on the interfacial activation energy.

3.1.3 Increase in interfacial impedance. The increase in interfacial impedance is usually attributed to the presence of the space charge layer. Experimental studies also support this conclusion (Fig. 6).

Haruyama *et al.* employed EIS to investigate the impact of the space charge layer at the interface between oxide cathodes and sulfide electrolytes. Their findings indicated that the presence of the space charge layer significantly increased interfacial resistance, thereby limiting the lithium-ion transport efficiency.[31,68] Brogioli *et al.* studied the interface between lithium–lanthanum–zirconate (LLZO) ceramic particles and PEO-based polymer electrolytes. They utilized theoretical calculations and experimental validation to demonstrate that the space charge layer at the LLZO/PEO interface made a substantial contribution to the interfacial resistance. By developing an electric double-layer model, they analyzed the charge distribution and potential difference at the interface and

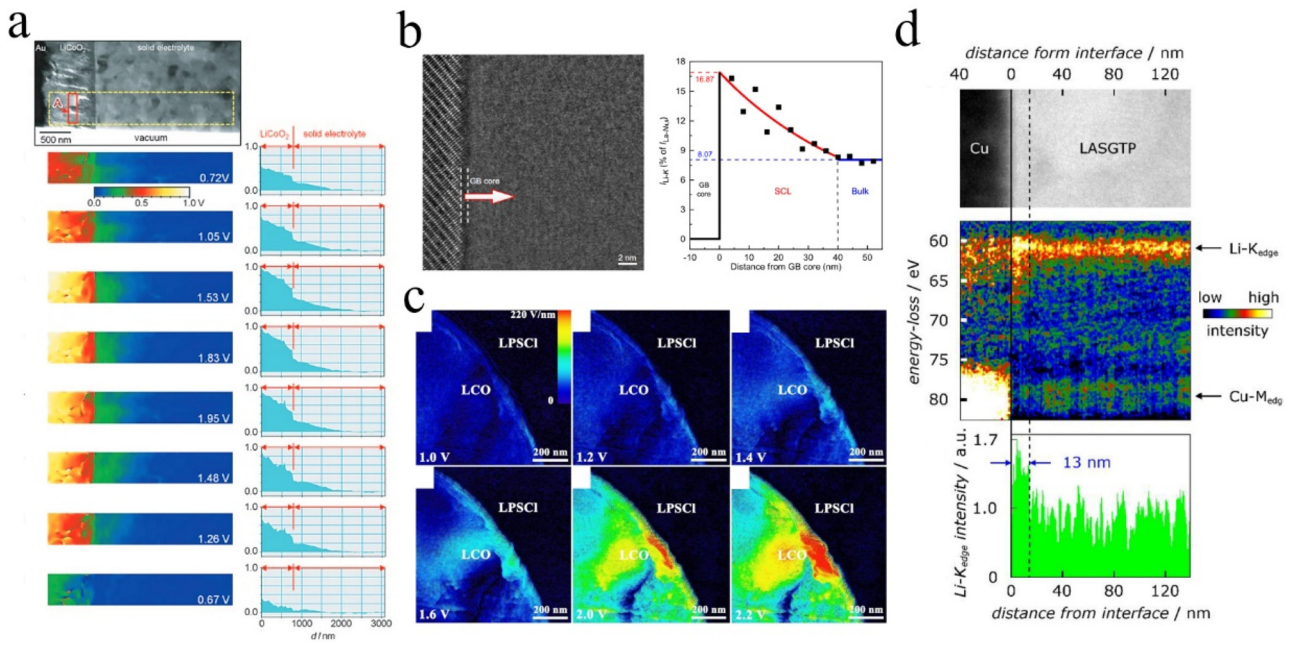

Fig. 4 Changes and imbalances in lithium-ion concentration: (a) Electric potential distribution around the $LiCoO_2$/electrolyte interface during the charge–discharge process. Reproduced under terms of the CC-BY license.[61] Copyright 2010, John Wiley and Sons. (b) Lithium-ion distribution near grain boundary cores. Reproduced under terms of the CC-BY license.[62] Copyright 2023, Zhenqi Gu *et al.*, published by Springer Nature. (c) Trends of electric field at different voltages at the LCO and LPSCL interfaces. Reproduced under terms of the CC-BY license.[50] Copyright 2020, Longlong Wang *et al.*, published by Springer Nature. (d) Li-ion distribution acquired at Cu/LASGTP interface from SR-EELS. Reproduced with permission.[49] Copyright 2019, John Wiley and Sons.

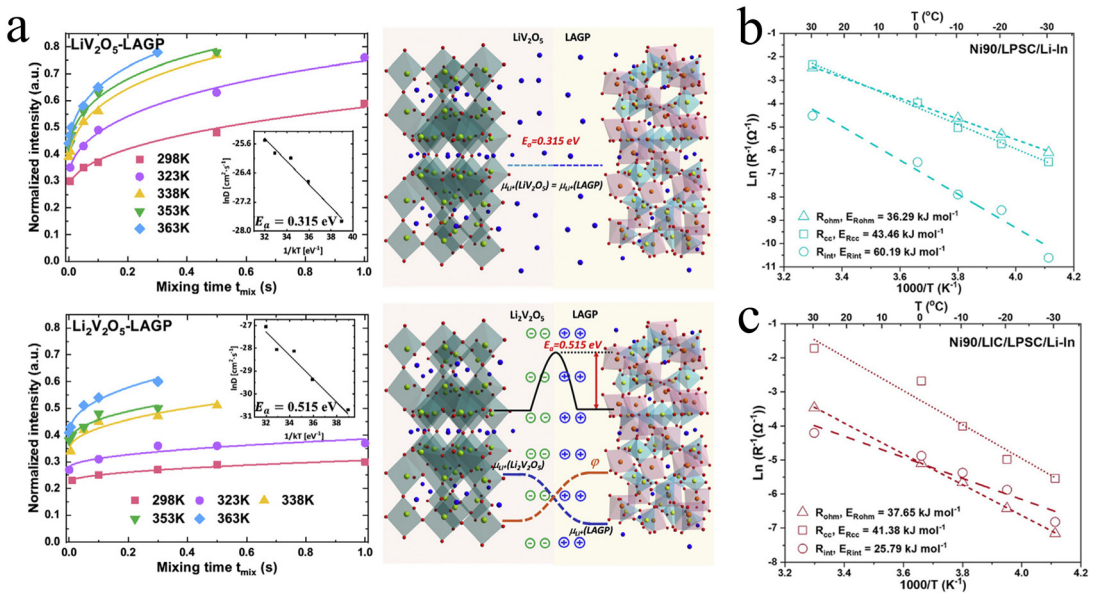

Fig. 5 The effect of SCL at interfaces on activation energy and impedance: (a) Determination of the activation energy of Li-ion exchange and schematic of space charge layer effects on Li-ion transport. Reproduced with permission.[32] Copyright 2020, Elsevier. (b,c) Arrhenius relationships of ohmic resistance (R_{ohm}), composite cathode resistance (R_{cc}), and interface resistance (R_{int}) to the operation temperatures for (b) Ni90/LPSC/Li–In, reproduced with permission.[66] Copyright 2024, American Chemical Society. (c) Ni90/LIC/LPSC/Li–In ASSBs. Reproduced with permission.[66] Copyright 2024, American Chemical Society.

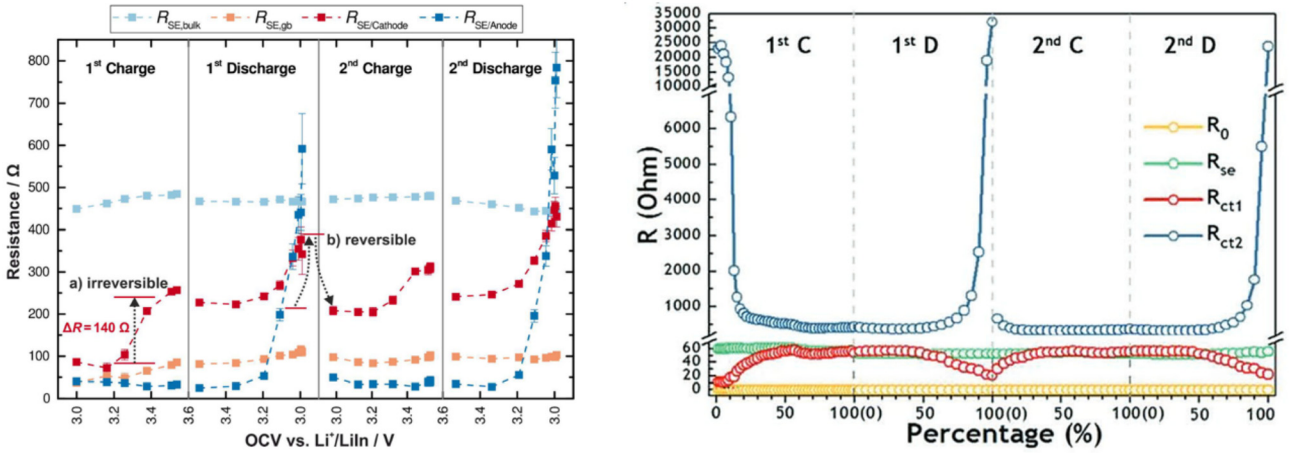

Fig. 6 Relationship between interfacial impedance and SOC. Reproduced with permission.[67] Copyright 2017, American Chemical Society. Reproduced with permission.[20] Copyright 2019, John Wiley and Sons.

derived the relationship between interfacial capacitance and potential difference. The experimental results revealed that the interfacial resistance varied with the concentration of lithium salts and reached a minimum value at high concentrations.[63]

3.1.4 Built-in electric field. The formation of the space charge layer is essentially an external manifestation of changes in the electronic band structure of the electrodes and electrolytes. Studies have demonstrated that the space charge layer can induce band bending and the generation of a built-in electric field, thereby influencing the transport of lithium ions (Fig. 7). For example, Yamamoto *et al.* utilized electron holography (EH) to directly observe the potential distribution in all-solid-state lithium-ion batteries during charge–discharge processes and found that the formation of the electric double layer led to a significant potential drop and a gradually extending spatial gradient. This alteration in potential distribution reflects the modification of the band structure, which further affects the lithium-ion transport kinetics. In addition, Fingerle *et al.* employed X-ray photoelectron spectroscopy (XPS) to investigate the chemical and electronic structure of the interface between $LiCoO_2$ and LiPON and identified a potential gradient at the interface. This potential gradient not only influences lithium-ion transport but may also facilitate electron transfer, potentially affecting interface stability.[47] The research by Hikima *et al.* utilized *in situ* hard X-ray photoelectron spectroscopy (HAXPES) to directly observe the changes in the electronic structure of Li_2MnO_3 electrodes during charge–discharge processes, revealing the impact of band bending on the interface reaction mechanism.[33] Band bending can lead to charge accumulation at the interface, thereby affecting the interface stability. At the Li_2MnO_3/LASGTP interface, the absence of an obvious reaction layer formation was observed, suggesting that band bending may, to some extent, inhibit the occurrence of interface reactions. The Li_2MnO_3 thin film in this study exhibited high discharge capacity and good cycling stability in all-solid-state batteries, potentially implying that the band bending caused by the space charge layer might, to some extent, be conducive to interface integrity. This effect is contingent upon the band structure of the interface. Although band theory primarily focuses on electrons rather than lithium ions, it remains a valuable tool for understanding interface evolution and characteristics.

3.2 SCL-dominated degradation mechanism

The formation of the space charge layer introduces complexities to interface issues. How, then, does the space charge layer accelerate interface degradation during the charge–discharge process of the battery? This section aims to explain the evolution of the space charge layer during the charge–discharge process from the perspective of band theory. Initially, upon interface formation, if the chemical potentials on both sides of the interface are identical, no space charge layer will form. This implies that the respective energy bands of the two materials at the interface will not bend, and no built-in electric field will be generated. However, when the chemical potentials of the two materials at the interface differ, the space charge layer will indeed form. Following the formation of the space charge layer, the interfacial activation energy increases, and the formation energy of lithium vacancies also increases, making it more energetically unfavorable for lithium ions to detach from one side of the interface and migrate to the other. This phenomenon is ultimately reflected in electrochemical measurements as increased interfacial impedance, leading to the degradation of battery performance.

As the battery commences charging and discharging, lithium ions are continually intercalated and deintercalated within the cathode and anode, leading to a continuous shift in the Fermi level of the cathode.[70] The Fermi level, representing the energy level with a 50% probability of electron occupation, also reflects the electron density of the material. During charging, as lithium ions are progressively extracted from the cathode, an equivalent number of electrons also leave, causing the Fermi level of the cathode to decrease correspondingly.

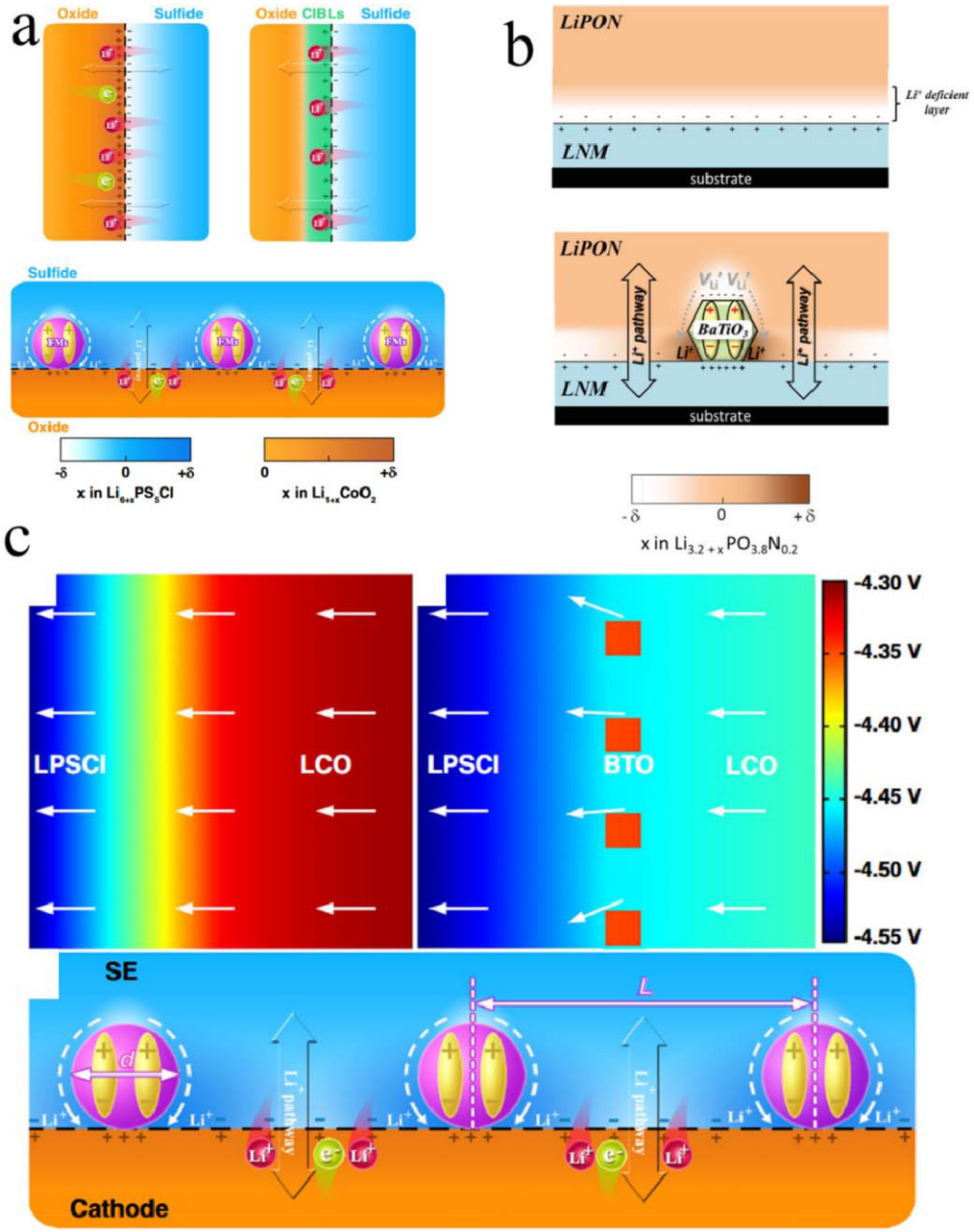

Fig. 7 The effect of ferroelectric materials on the interfacial SCL: (a) Schematic illustration of interface charge redistribution between oxide cathodes and sulfide SEs after different interface engineering approaches. Reproduced under terms of the CC-BY license.[50] Copyright 2020, Longlong Wang *et al.*, published by Springer Nature. (b) Schematic views of Li+ concentration profile in LiPON at open circuit conditions around a pristine LiPON/LNM interface. Reproduced with permission.[69] Copyright 2014, John Wiley and Sons. (c) FEM simulations of the effects of BTO nanocrystals. Reproduced under terms of the CC-BY license.[50] Copyright 2020, Longlong Wang *et al.*, published by Springer Nature.

This process induces a Fermi level mismatch across the interface. This mismatch results in the bending of the conduction band minimum and valence band maximum of both the cathode and the electrolyte and, consequently, to a dynamically evolving SCL (Fig. 8).

During electrochemical cycling, the relative dominance of chemical and mechanical degradation at solid–solid interfaces is strongly dependent on the state of charge (SOC), rather than being governed by a single universal failure mechanism. As lithium ions are continuously intercalated and deintercalated, the Fermi level of the cathode dynamically shifts, reflecting changes in both lithium content and electronic structure.[70] This evolution leads to a SOC-dependent electrochemical potential mismatch across the cathode–electrolyte interface and, consequently, to a dynamically evolving SCL. At relatively low to moderate voltages, particularly for layered Ni-rich cath-

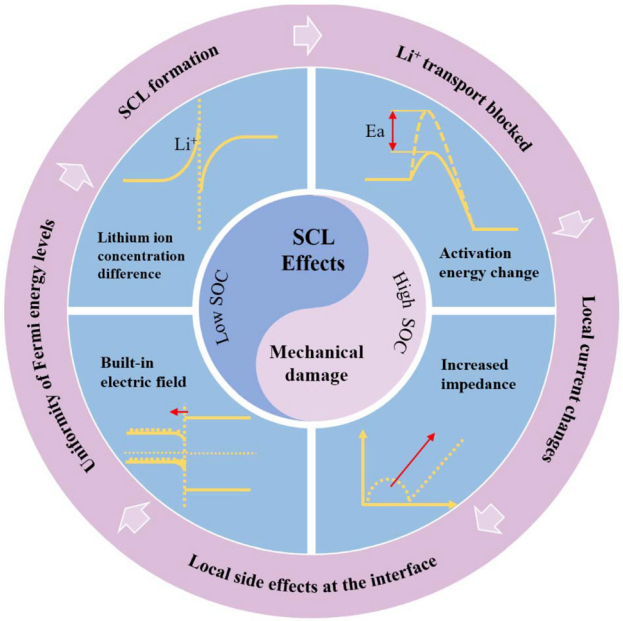

Fig. 8 SCL-dominated degradation mechanism.

odes, the overall volumetric change of the cathode is comparatively limited, and interfacial mechanical contact can generally be maintained under typical stack pressures. In this regime, the electrochemical potential mismatch between the cathode and solid electrolyte remains significant, giving rise to pronounced band bending and a steep interfacial electric potential gradient. Under such conditions, the SCL plays a dominant role in interfacial degradation by locally redistributing lithium ions and charge carriers. The resulting strong internal electric fields can accelerate parasitic interfacial reactions, promote electrolyte decomposition, and induce the formation of lithium-rich or lithium-depleted regions. Importantly, the interphase products generated through these SCL-driven processes further modify the local chemical potential landscape and electric field distribution, thereby increasing interfacial heterogeneity and reinforcing chemical degradation pathways. As the SOC increases toward higher voltages, however, the degradation priority may shift. For Ni-rich cathodes, anisotropic lattice expansion and contraction become more pronounced at high degrees of delithiation. If the externally applied stack pressure is insufficient or spatially non-uniform, even a relatively narrow SOC window can trigger mechanical degradation, such as interfacial cracking, contact loss, or partial delamination. In this high-voltage regime, mechanical failure can locally disrupt ionic transport pathways and dominate interfacial degradation. Moreover, under certain SOC conditions, the electrochemical potentials across the interface may approach equilibrium, reducing the driving force for further SCL-induced charge redistribution. In such cases, SCL-related electrostatic effects no longer serve as the primary degradation origin, although they may still modulate local reaction kinetics at damaged regions. Hikima *et al.*'s *in situ* study on band structure changes revealed interface alterations in all-solid-state batteries.[33] As depicted in Fig. 9b, significant band bending occurs at the cathode–electrolyte interface towards the end of discharge. More critically, the built-in electric field generated by the bending of the cathode's energy bands aligns with the external electric field applied during charging, potentially exacerbating band bending. The generated built-in electric field promotes the redistribution of lithium ions, leading to the formation of lithium-rich or lithium-poor regions. Zhang *et al.*[20] studied the periodic evolution process of interfaces in all-solid-state batteries and established a model of the relationship between lithium-ion concentration at the interface and battery status. The model results show that during charging, lithium ions accumulate on the positive electrode side. During discharge, the distribution of lithium ions shows a trend opposite to that during charging. The blockage of lithium-ion transport channels can result in localized charge density inhomogeneities, rendering the interface more susceptible to physical or chemical transformations and consequently altering the interface composition. This, in turn, leads to further changes in the Fermi level. This cycle repeats continuously throughout the charge–discharge process, macroscopically manifesting as a gradual decline in battery performance, increased impedance, and interface degradation. Moreover, the volume changes in the Ni-rich cathode during cycling can cause the formation of mechanical contact failure at the cathode–electrolyte interface, potentially interrupting lithium-ion transport pathways and leading to an increase in local interfacial lithium-ion concentration. At high voltages, valence band electrons in the electrolyte may gain sufficient energy to transition to the conduction band, generating electron–hole pairs. Electrons excited to the conduction band, possessing higher energy, tend to migrate from the conduction band of the electrolyte to the conduction band of the cathode due to the cathode's higher conduction band energy position, as electrons move towards regions of higher potential. This electron migration causes the electrolyte to lose electrons and undergo oxidation reactions, further degrading the interface. Furthermore, the side reaction products formed due to the space charge layer during a charge–discharge cycle are often not fully reversible. Over multiple cycles, this leads to irreversible degradation of the interface and a corresponding decline in battery performance.[71]

Overall, the space charge layer (SCL) at solid–solid interfaces in all-solid-state batteries should be understood as a dynamic and SOC-dependent interfacial phenomenon that continuously evolves during charge–discharge cycling. As lithium ions are repeatedly intercalated and deintercalated, the interfacial electrochemical potential mismatch and band alignment are periodically reconstructed, leading to the recurrent formation, relaxation, and redistribution of the SCL. This cyclic evolution gives rise to persistent lithium-ion accumulation or depletion at the interface, locally modifying ion transport pathways and electrostatic environments. Over extended cycling, such repetitive SCL reconstruction acts as a feedback loop that progressively amplifies interfacial heterogeneity,

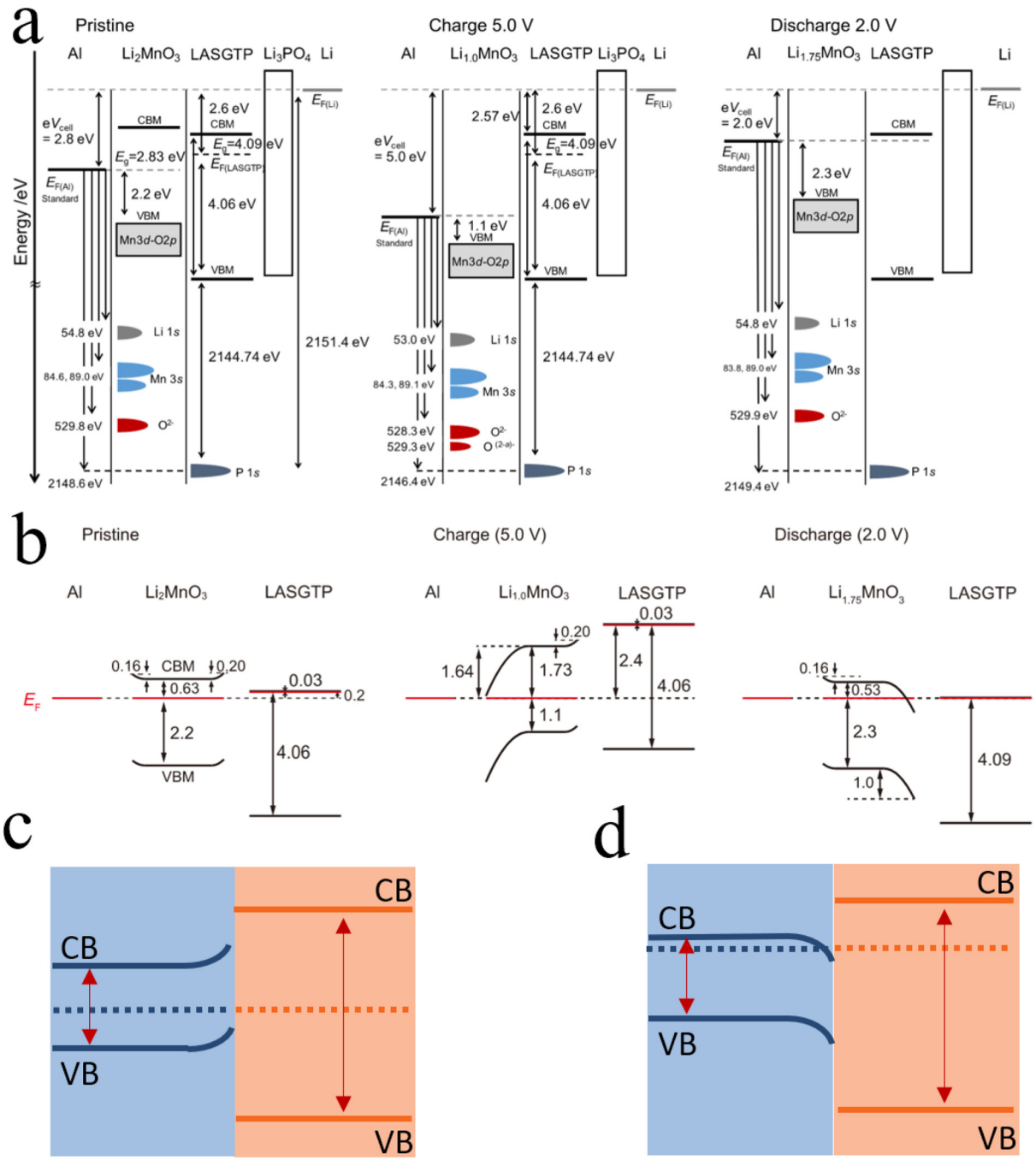

Fig. 9 Band structure changes of all-solid-state batteries during cycling. (a) Band structure changes of all-solid-state batteries during cycling. Reproduced under terms of the CC-BY license.[33] Copyright 2022, Kazuhiro Hikima *et al.*, published by Springer Nature. (b) Band bending of the cathode side with additional assumptions represented by the relative energy level positions. Reproduced under terms of the CC-BY license.[33] Copyright 2022, Kazuhiro Hikima *et al.*, published by Springer Nature. (c and d) Schematic of the energy bands at the interface of LMO and LASGTP at both 5 V and 2 V.

resulting in increased impedance and gradual performance degradation. Importantly, the relative contributions of chemical and mechanical degradation associated with SCL evolution are strongly dependent on the state of charge. At low to moderate SOC ranges, where volumetric changes of electrode materials are comparatively limited and interfacial contact is largely preserved, SCL-induced electrostatic effects tend to dominate. In this regime, steep interfacial potential gradients can hinder lithium-ion transport and promote parasitic chemical reactions, such as electrolyte decomposition or interphase growth, which further alter the local chemical potential and reinforce SCL evolution. By contrast, at high SOCs, anisotropic

lattice strain and accumulated stress may trigger mechanical degradation, including contact loss or interfacial delamination, particularly under insufficient or non-uniform stack pressure. In such cases, mechanical failure can become the primary degradation origin, while the SCL plays an amplifying role by intensifying local electric fields and accelerating chemical reactions at damaged regions. Under certain SOC conditions, partial equilibration of interfacial electrochemical potentials may also reduce the direct driving force for further SCL growth, shifting the degradation priority away from electrostatic effects.

These considerations demonstrate that chemical and mechanical degradation processes at solid–solid interfaces are not independent phenomena but are inherently coupled through SOC-dependent interfacial electrostatics and structural evolution. While many existing studies focus on either chemical or mechanical degradation in isolation, such an approach is insufficient to fully capture the dynamic nature of SCL-governed interfaces. A comprehensive understanding of interfacial degradation in all-solid-state batteries therefore requires integrated electro–chemo–mechanical frameworks that explicitly incorporate SOC-dependent band alignment, space charge evolution, and stress–strain coupling. Developing such coupled models, together with advanced *operando* characterization techniques, will be essential for decoupling these intertwined mechanisms and for guiding rational interface design strategies.

Notably, emerging evidence suggests that under specific material combinations and interfacial architectures, the SCL can actively promote or facilitate lithium-ion transport. Wang *et al.*[72] reported the formation of a fast ion-conducting interfacial region at the LYC–LZC interface, where the SCL was proposed to facilitate enhanced lithium-ion mobility. Similar enhancements in ionic conductivity have been observed in mixed-phase electrolyte systems reported by Ohta *et al.*,[34] suggesting that appropriately engineered SCLs can function as ion-transport-promoting interfacial channels. These findings collectively indicate that the role played by the SCL in all-solid-state batteries is not intrinsically detrimental or beneficial but is governed by a complex interplay of interfacial electrostatics, materials chemistry, mechanical integrity, and operating conditions. A comprehensive understanding of SCL effects therefore requires advanced characterization techniques and physically informed modeling approaches capable of decoupling these intertwined factors across multiple time and length scales. More detailed discussions of characterization strategies and control methodologies are provided in the following sections.[73–75]

4. Characterization methods

A significant factor hindering the progress in studying the space charge layer is the lack of robust characterization methods. Given the internal location of the all-solid-state battery interface, conventional characterization and testing techniques often fall short of providing in-depth information regarding its microscopic morphology or distribution. Furthermore, the prevalent use of mixed composite cathodes in current designs further complicates the characterization of the space charge layer in these batteries.[19,58,62,73,76–79] The primary challenges in characterizing the space charge layer can be summarized as follows:

First, the microscopic-scale characteristics of the space charge layer pose a considerable difficulty. Typically existing at the atomic or nanoscale, its thickness can be limited to just a few nanometers or even less. But the majority of currently available characterization techniques are capable of providing only macroscopic or localized information, making it challenging to fully and quantitatively elucidate the microscopic structure and ion transport characteristics of the space charge layer. For instance, the widely used EIS can indirectly indicate changes in interfacial impedance but cannot directly visualize the microscopic structure of the space charge layer. X-ray photoelectron spectroscopy (XPS), while effective at analyzing the valence states and chemical composition of elements at the interface, lacks the ability to quantitatively describe the distribution of lithium ions. Existing characterization techniques face difficulties in directly observing and measuring the distribution and concentration changes of lithium ions at such minute scales. Conventional transmission electron microscopy (TEM), despite its high resolution, still encounters limitations in directly imaging the space charge layer and necessitates specialized sample preparation.

Second, the inherent complexity of the interface presents another major hurdle. The space charge layer forms at the solid–solid interface between the electrode and the electrolyte, where a multitude of intertwined physical and chemical phenomena may occur, including interface reactions, element diffusion, and interface side reactions. These interconnected processes make it difficult to isolate the specific impact of the space charge layer for individual analysis. Interface reactions, for example, can lead to the formation of new phases, further altering the electrochemical properties of the interface and potentially obscuring the intrinsic characteristics of the space charge layer. Moreover, the vast array of electrode and electrolyte materials utilized in all-solid-state batteries results in significant variations in the interface characteristics formed by different material combinations. The formation mechanism and influencing factors of the space charge layer are material-dependent, thus complicating the establishment of a universally applicable characterization model.

Third, the dynamic change characteristics of the space charge layer add another layer of complexity. The formation and evolution of the space charge layer are dynamic processes, and its properties fluctuate with the battery's charging and discharging cycles, as well as variations in temperature, pressure, and other operational conditions. The space charge layer within the battery may undergo continuous changes during operation, rendering it challenging to capture its complete behavior using static characterization techniques. Advanced

in situ characterization methods are likely required to better understand its dynamic evolution.

Fourth, interface contact and stability issues further complicate the characterization efforts. The contact between the solid electrolyte and the electrode is often not perfectly intimate, potentially resulting in pores, cracks, and other defects at the interface. These imperfections can affect the formation and distribution of the space charge layer and also increase the difficulty of accurate characterization. Mechanical instability at the interface can lead to localized alterations in the space charge layer, potentially compromising the accuracy of the characterization results.

The challenge in characterizing the space charge layer in all-solid-state batteries arises from the synergistic effect of various factors, including its microscopic scale, interface complexity, dynamic nature, and interface contact and stability issues. These factors are intricately intertwined, contributing to the slow progress in the study of the space charge layer. However, the continuous advancement and application of sophisticated characterization techniques offer promising avenues to overcome this bottleneck.[80] In particular, *in situ* characterization techniques hold significant potential as they can monitor the dynamic changes of the space charge layer in real time during battery operation, providing crucial insights into its formation mechanism and influencing factors. Takada's early work involved increasing the potential difference between the oxide cathode and the sulfide solid electrolyte to investigate the impact of the space charge layer effect on battery performance, demonstrating that the effect is primarily attributable to interface mismatch.[31] However, finer characterization of the space charge layer remained limited by the available techniques at the time. Thanks to technological progress, researchers have since reported significant advancements in high-precision characterization instruments. For instance, Gu *et al.* successfully captured the charge distribution at the interface using high-resolution aberration-corrected electron microscopy, revealing a lithium-ion aggregation zone rather than the lithium-ion depletion zone previously reported in the literature.[62] This finding underscores the indispensable role played by advanced characterization techniques in understanding interface evolution. Current research methodologies for studying the space charge layer predominantly involve simulation calculations and experimental characterization.

4.1 Simulation and calculation

First-principles calculations and density functional theory (DFT) are increasingly employed to provide atomic-level insights into defect formation energies, electronic band alignment, and potential distribution at the electrode–solid electrolyte interface (Fig. 10).[52,79,81–85] These methods can predict the interfacial potential drop driven by electron transfer and the space charge layer of Li^+, as well as how these potential drops vary with the state of charge (SOC) of the battery. More sophisticated interface models have been developed beyond simple equilibrium conditions, considering factors such as applied voltage, temperature, and specific properties of the electrode and electrolyte materials (*e.g.*, dielectric constant) that influence the formation of the space charge layer and its impact on lithium-ion transport. These models reveal that the size of the space charge layer in solid electrolytes may be larger than that in liquid electrolytes and is strongly dependent on the dielectric properties of the materials. It has been recognized that the properties of the space charge layer (thickness, ion concentration, potential drop) are dynamic and depend on the SOC of the battery and the crystal orientation of the materials, which affect the defect formation energies and band alignment at the interface.[86]

For instance, in 2017, Fingerle *et al.* utilized DFT modeling to evaluate the defect concentration and Fermi level position at the interface between $LiCoO_2$ and LiPON to elucidate the formation mechanism and evolution of the space charge layer.[47] The modeling results showed consistency with the actual interface, indicating that the formation of the space charge layer arose from the equilibrium of the electrochemical potential of Li ions at the interface. This phenomenon persisted even after annealing, suggesting that the electrochemical potential gradient at the interface is intrinsic. Swift and Qi proposed a first-principles-based model to predict the potential distribution in all-solid-state lithium batteries (ASSLBs) and applied it to the Li/LiPON/Li_xCoO_2 system.[87,89] The model incorporated the interfacial potential drop resulting from lithium-ion transport and electron transfer and integrated defect formation energy calculations to predict the formation of the SCL, thereby forecasting the migration direction of lithium ions within the space charge layer. Their study demonstrated that the formation and interfacial potential energy of the space charge layer are dependent on the SOC of the cathode material, specifically the concentration of lithium ions in the cathode. De Klerk *et al.* employed a simplified model to evaluate the interfacial capacitance and resistance of the SCL in typical electrode–electrolyte combinations, applying it to the contact of $LiCoO_2$ (LCO) and graphite electrodes with LLZO and LATP solid electrolytes.[35,54] Their findings suggested that the thickness of the SCL is typically at the nanoscale, and the resistance to Li^+ transport is negligible unless a completely depleted Li^+ layer is formed in the solid electrolyte. This implies that the impact of the SCL on the performance of all-solid-state batteries is minor, and the primary causes of large interfacial resistance are poor contact between the electrode and the electrolyte, decomposition products, *etc*. The model's validity was supported by comparisons with experimental results, and the authors acknowledged some assumptions and uncertainties within the model, such as the simplified treatment of Coulomb interactions. Liu *et al.* proposed a novel equivalent circuit model that considers the interface to encompass not only capacitance but also space charge layer resistance and polarization resistance.[79] The elements of the circuit model were quantified based on the improved Planck–Nernst–Poisson (MPNP) model. This new model offers a better explanation for the real impedance tail observed in the low-frequency region. The validity of the model was corroborated by

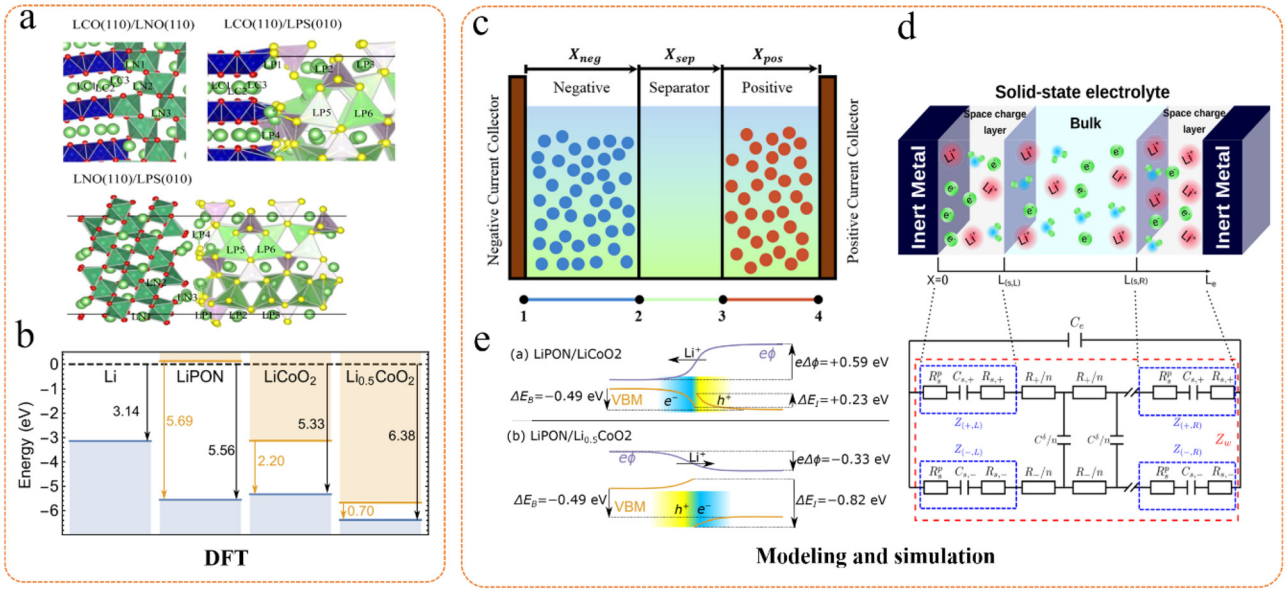

Fig. 10 Application of DFT and model simulations in the space charge layer. (a) Different sites on the contact surfaces of LCO, LPS, and LNO. Reproduced with permission.[31] Copyright 2014, American Chemical Society. (b) The vacuum-aligned position of the electronic bands in lithium metal, LiPON, $LiCoO_2$, and $Li_{0.5}CoO_2$ before contact. Occupied bands (VBM) are blue and unoccupied bands (CBM) are orange. Vacuum (dashed line) alignments and band gaps are indicated. Reproduced with permission.[87] Copyright 2019, John Wiley and Sons. (c) Schematic representation of three domains in P2D model. Reproduced with permission.[88] Copyright 2022, Elsevier. (d) Schematic of a metal/electrolyte/metal cell with the space charge layers at the interface and the proposed equivalent circuit model. Reproduced with permission.[79] Copyright 2021, American Chemical Society. (e) Schematic of the electrostatic potential and valence bands at the interfaces between LiPON and Li_xCoO_2 for x = 1 and x = 0.5. Reproduced with permission.[87] Copyright 2019, John Wiley and Sons.

comparisons with experimental results. Their study revealed that polarization resistance plays a significant role in the low-frequency region, particularly in solid electrolytes exhibiting non-ideal electron blocking. The model's accuracy was verified by comparison with the experimental impedance spectrum of LiPON, and the influence of temperature on ionic conductivity was discussed, further enhancing the understanding of solid electrolyte impedance. Moreover, Al-Ali *et al.* introduced a deep learning-based algorithm utilizing convolutional neural networks (CNN) and long short-term memory networks (LSTM) to identify the circuit model that best fits the measured impedance spectra.[90] A two-stage optimization technique was also proposed to determine the optimal circuit model parameters. The efficacy of the proposed algorithm was validated using experimental impedance data from NiMH batteries and cherry tomato bioimpedance. The results indicated that the algorithm could successfully model and fit the given impedance data with low error, demonstrating its significant value for accurately identifying interfacial impedance. Regarding the dynamic evolution of the space charge layer, Katzenmeier *et al.* employed kinetic Monte Carlo (kMC) simulations to investigate the SCL phenomenon in solid electrolytes, aiming to predict the spatial extent of the SCL with a minimal number of input parameters and explore its temporal evolution.[64,65,81] They constructed a kMC model to simulate the hopping mechanism of Li^+ ions within the solid electrolyte, studied the formation process of the SCL, and validated the simulation results with experimental data. The kMC simulation results exhibited good agreement with the experimental findings, capturing the physical behavior of SCL formation and revealing the impact of material properties, such as Li^+ ion concentration and dielectric constant, on the thickness and asymmetry of the SCL. The accuracy of the kMC model in predicting SCL thickness and capacitance was confirmed by comparison with experimental data.

The research conducted by these scholars underscores the considerable significance of model simulation and first-principles calculations in elucidating the formation and evolution mechanisms of the space charge layer. However, the accuracy of these models and calculation results necessitates experimental verification, highlighting the indispensable role played by experimental studies.[88,90–98]

4.2 Experimental characterization

In experimental validation, the synergistic application of advanced characterization techniques provides multidimensional data to support theoretical models (Fig. 11).[100,104–112] X-ray photoelectron spectroscopy (XPS) can be employed for the quantitative analysis of the evolution of elemental chemical states at the interface. By comparing the shifts in the binding energies of Li 1s and transition metal 2p orbitals at varying depths, the direction of electron transfer predicted by DFT and the lithium-ion concentration gradient within the SCL can be verified. Transmission electron microscopy (TEM),

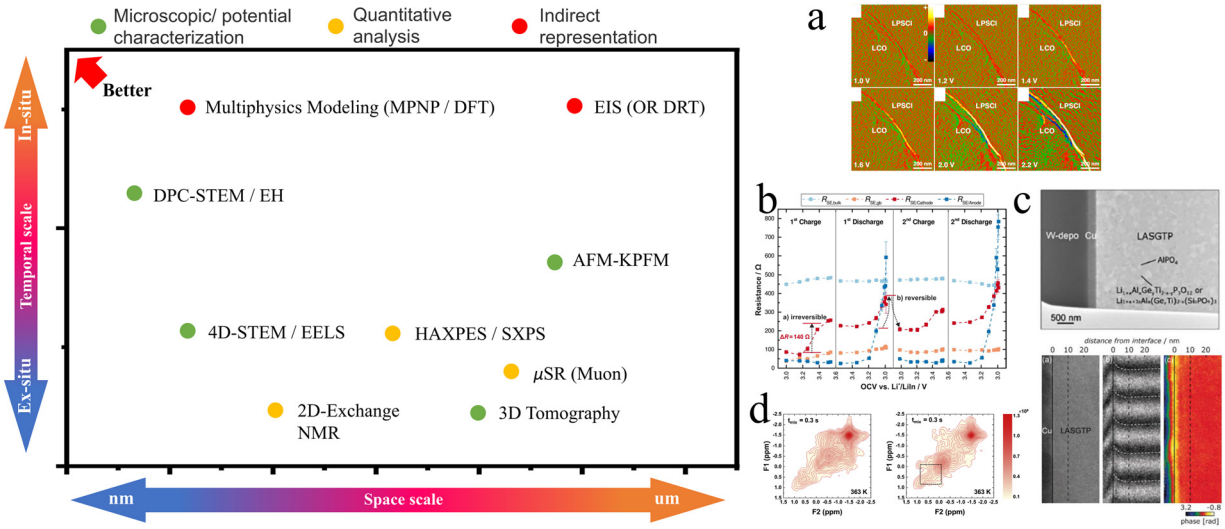

Fig. 11 Currently commonly used methods for characterizing the space charge layer and their advantages on both spatial and temporal scales.[20,32,49,50,54,60,61,71,74,76,77,79,80,82,88,98–104] (a) *In situ* charge-density-distribution characterization of the LCO/LPSCl interface. Reproduced under terms of the CC-BY license.[50] Copyright 2020, Longlong Wang *et al.*, published by Springer Nature. (b) Evolution of the four resistances obtained by fitting the impedance spectra. Reproduced with permission.[67] Copyright 2017, American Chemical Society. (c) Electric potential distribution near Cu/LASGTP interface obtained from phase-shifting electron holography. Reproduced with permission.[49] Copyright 2019, John Wiley and Sons. (d) Exchange phenomenon within LiV_2O_5 and $Li_2V_2O_5$ bulk, ^{6}Li 2D exchange NMR spectrum of LiV_2O_5-LAGP and $Li_2V_2O_5$-LAGP at 363 K with 0.3 s mixing time. Reproduced with permission.[32] Copyright 2019, Elsevier.

often coupled with electron energy loss spectroscopy (EELS), enables nanoscale resolution of interface structure analysis. Notably, *in situ* observation of beam-sensitive regions *via* electron beam irradiation allows for the direct measurement of the actual thickness of the lithium-depleted layer, which can be statistically correlated with the extent of lattice distortion calculated by DFT. Furthermore, to overcome the spatial averaging limitations of conventional 2D TEM projections, 3D electron tomography has emerged as a cutting-edge approach. By reconstructing a series of 2D images acquired at different tilt angles, 3D electron tomography, often combined with EDS or EELS, provides a holistic view of the spatial heterogeneity of the SCL and its coupling with the cathode–electrolyte interphase (CEI). This 3D perspective is crucial for identifying non-uniform Li-ion percolation pathways in bulk-type composite electrodes where the SCL effects are influenced by complex local geometries. Synchrotron X-ray absorption spectroscopy (XAS) facilitates the dynamic tracking of changes in the oxidation states of transition metals at the interface during battery cycling, revealing the impact mechanism of the space charge layer effect on the structural stability of the cathode material. For example, Fingerle *et al.* integrated surface science methods and simulation calculations to investigate the reaction and space charge layer formation at the interface between $LiCoO_2$ and lithium phosphorus oxynitride (LiPON).[47] Utilizing XPS, synchrotron X-ray photoelectron spectroscopy (SXPS), and ultraviolet photoelectron spectroscopy (UPS), they meticulously detailed the chemical reactions and charge transfer processes occurring at the interface. XPS and SXPS can accurately monitor alterations in the valence states and chemical environment of elements at the interface, while UPS serves to measure the work function and valence band structure, thereby constructing a comprehensive band structure diagram. Yamamoto *et al.* employed quantitative electron holography (EH) to directly observe the potential distribution changes induced by lithium-ion diffusion in all-solid-state LIBs, revealing the lithium-ion potential distribution at the cathode/solid electrolyte interface during charge–discharge reactions.[49,61] Complementing electron-based techniques, the combination of *in situ* Atomic Force Microscopy (AFM) and Kelvin Probe Force Microscopy (KPFM) offers a powerful platform for mapping the internal potential profiles of cross-sectioned solid-state cells. KPFM measures the contact potential difference (CPD) between a conductive tip and the sample surface with high spatial and voltage resolution, allowing for the direct visualization of the electric potential drop across the SCL. For instance, Masuda *et al.*[100] utilized *in situ* KPFM to map the potential distribution within a charged all-solid-state LIB, successfully identifying the local overpotential at the cathode/electrolyte interface and quantifying the width of the resistive space-charge region under operative conditions. Electrochemical impedance spectroscopy serves as a critical verification tool. By establishing an equivalent circuit model that incorporates the impedance of the space charge layer (*e.g.*, introducing a parallel combination of a Warburg diffusion element and interfacial capacitance), the contribution of the SCL to the lithium-ion migration barrier can be quantitatively separated. Yu *et al.* utilized EIS and solid-state nuclear magnetic resonance (NMR) techniques to study lithium-ion transport characteristics in $Li_7P_3S_{11}$ sulfide-based solid electro-

lytes.[60] EIS was used to measure the ionic conductivity of the electrolyte and to determine the activation energy for lithium-ion transport. Gu *et al.* combined high-angle annular dark-field scanning transmission electron microscopy (HAADF-STEM), EELS, and *ab initio* molecular dynamics (AIMD) simulations to investigate the atomic configuration and ion transport behavior of the SCL in LLTO.[62] Their findings indicated that the SCL in LLTO is actually a lithium-ion-rich region. The lithium ions within the SCL primarily occupy the 3c interstitial sites, and their ion transport efficiency is comparable to that of the bulk phase, suggesting that the SCL is not the primary cause of the large grain boundary resistance. On the contrary, the grain boundary core with lithium-ion depletion is the main bottleneck for the high grain boundary resistance in LLTO. Wang *et al.* utilized *in situ* differential phase contrast scanning transmission electron microscopy (DPC-STEM) to directly observe the net charge density distribution at the $LiCoO_2/Li_6PS_5Cl$ interface in sulfide-based all-solid-state batteries.[50] DPC-STEM technology can monitor the accumulation of lithium ions at the interface in real time, thereby revealing the hindrance effect of the SCL on lithium-ion transport at the interface. Recent advances in 4D-STEM have further enhanced this capability, enabling the simultaneous mapping of local crystallinity, strain, and electric fields, which provides a more nuanced understanding of how structural degradation at the NMC/LGPS interface correlates with SCL formation.[20,101] Isaac *et al.* employed EIS to investigate ion charge transport and transfer in multilayer model systems based on polyethylene oxide (PEO) polymer electrolytes and NaSICON-type ceramic electrolytes.[99] Their study found that the total polarization resistance (R_p) of the multilayer system can be decomposed into the sum of the bulk electrolyte migration resistance (R_{el}), the interfacial charge transfer resistance (R_{ct}), and the diffusion resistance (R_{dif}), *i.e.*, $R_p = R_{el} + R_{ct} + R_{dif}$. This indicates that EIS can quantitatively analyze changes in interfacial impedance by decomposing the raw data. Utilizing Li NMR technology, researchers can quantitatively analyze the diffusion coefficient and transport barrier of lithium ions in the solid electrolyte, as well as the lithium-ion transport characteristics at the electrode–electrolyte interface.[32,101,113] Compared with conventional spectroscopic and electrochemical methods, these emerging techniques provide unprecedented spatial dimensionality and *operando* sensitivity, enabling direct correlation between electrostatic potential evolution, local lithium redistribution, and interfacial structural degradation.

Looking ahead, the development and application of more sophisticated *in situ* characterization techniques will hopefully lead to a more comprehensive understanding of the microscopic structure and mechanism of action of the space charge layer. This, in turn, will provide a robust theoretical foundation for the interface optimization and performance enhancement of all-solid-state batteries. It is precisely through the reciprocal interplay between theoretical modeling and experimental validation that the true impact of the space charge layer on the interface of all-solid-state batteries can be elucidated.

Table 1 shows the statistical data on methods for characterizing space charge layers.

5. Space charge layer control strategies

Following an in-depth analysis of the formation mechanism of the SCL, characterization methods, and its multifaceted impact on the performance of all-solid-state batteries, it is clear that the space charge layer represents a key bottleneck limiting the achievement of high-performance and long-cycle-life applications for all-solid-state Ni-rich batteries.[114–117] Considering the substantial influence of the space charge layer on interfacial impedance, lithium-ion transport kinetics, chemical and mechanical stability, and overall battery performance, the exploration of effective control strategies to mitigate or overcome its detrimental effects is urgently warranted.[77,118–123]

Fig. 12 summarizes the prevailing approaches, including surface coating, bulk/gradient doping, and dielectric engineering. Although traditionally treated as distinct categories, these strategies can be mechanistically reorganized into two unified frameworks: Hierarchical Band Alignment Engineering and Interfacial Field Modulation. This classification better reflects the underlying physics governing SCL formation and supports the rational design of next-generation interface engineering strategies.

5.1 Hierarchical band alignment engineering

Hierarchical Band Alignment Engineering refers to a multi-level electronic-structure design strategy in which both the interfacial and bulk energy levels are tuned to create a continuous, graded alignment across the cathode–electrolyte interface. This framework consolidates surface coating and bulk/gradient doping into a single concept, as both ultimately regulate the electrochemical potential landscape that governs SCL formation.

5.1.1 Surface coating as interfacial band regulators. Surface coatings represent the first hierarchical level in Hierarchical Band Alignment Engineering, functioning as interfacial band-regulating layers that buffer the electronic mismatch between the cathode and the solid electrolyte. Their primary functions include not only traditional chemical passivation but also acting as interface band regulators. They reshape the interfacial energy landscape, modulate band bending, and smooth the electrochemical potential transition, thereby suppressing the formation intensity of the SCL.

Performance improvements associated with coatings have been widely demonstrated in Ni-rich batteries.[125–135] For example, Takada and Zhang *et al.* reported that $LiNbO_3$-coated NCM811 exhibits significantly lower interfacial resistance after cycling, confirming that appropriately selected coating layers can effectively weaken SCL-induced impedance growth.[136] Similarly, Liu *et al.* identified that LiI coatings improve lithium-ion transport across the interface by reducing SCL-

Table 1 Summary of methods for characterizing interfaces

Ref.	Characterization techniques	Key advantages	Limitations	Application scenarios
Al-Ali *et al.*[90] Isaac *et al.*[99] Liu *et al.*[79]	EIS	Sensitive to interfacial resistance and capacitance changes; non-destructive; suitable for *operando* analysis.	Indirect probe; model-dependent interpretation; limited spatial resolution.	Identifying SCL-induced interfacial impedance growth; tracking dynamic interfacial evolution during cycling.
Wang *et al.*[50]	*In situ* DPC-STEM	Directly visualizes net-charge-density and Li-ion accumulation at atomic scale.	Highly sensitive to electron beam; requires precise FIB sample preparation.	Visualizing charge distribution at high-voltage LCO/Li_6PS_5Cl interfaces.
Cheng *et al.*[32] Liu *et al.*[102] Yu *et al.*[60] Liu *et al.*[103] Yu *et al.*[54]	2D exchange NMR	Non-invasive; quantifies spontaneous Li-ion exchange rates and activation energy barriers.	Low spatial resolution; requires specific isotopes ($^6Li/^7Li$) for signal clarity.	Quantifying Li-ion transport barriers across $Li_xV_2O_5$/LAGP or S-based interfaces.
Nomura *et al.*[49] Yamamoto *et al.*[61]	Electron Holography (EH)	Direct observation of 2D electric potential maps and dynamic changes during (dis)charge.	Low signal-to-noise ratio; complex phase reconstruction; limited to thin-film models.	Mapping potential drops and SCL width in model all-solid-state thin-film batteries.
Masuda *et al.*[100]	*In situ* KPFM	High surface potential sensitivity; maps cross-sectional potential across the entire cell.	Surface-sensitive only; potential contamination from surface oxidation or humidity.	Analyzing potential distribution and local resistance in bulk-type solid-state cells.
Hikima *et al.*[33] Fingerle *et al.*[47] Hakari *et al.*[106]	*Operando* HAXPES/XPS	Probes electronic band structure and "band bending" to infer potential alignment.	Limited probing depth (nm scale); indirect evidence of SCL *via* energy level shifts.	Distinguishing between chemical decomposition layers and electrostatic SCLs.
Sugiyama *et al.*[98]	Low-energy muons (μSR)	Probes local magnetic fields and Li-ion dynamics at depth-tunable nanometer scales.	Requires synchrotron/accelerator facilities; extremely complex data interpretation.	Searching for Li-ion depletion layers in thin-film battery materials.
Feng *et al.*[104] Yu *et al.*[111] Zhang *et al.*[76] Isaac *et al.*[99]	EIS with DRT/TLM	Non-destructive; decouples overlapping processes (SCL, SEI, bulk) *via* relaxation times.	Model-dependent interpretation; lacks direct structural/spatial confirmation.	Monitoring the evolution of interfacial impedance during long-term cycling/aging.
Paranamana *et al.*[101] Zhang *et al.*[20]	4D-STEM/EDS	Provides structural and compositional maps of the interphase at the nanoscale.	Primarily captures chemical interphases (CEI) rather than pure electrostatic SCL.	Understanding the coupling between chemical reactions and charge distribution.
Wang *et al.*[50] Swift & Qi[87] Liu *et al.*[103] Brogioli *et al.*[63]	Multiphysics modeling (MPNP/DFT)	Predicts potential profiles, defect concentrations, and SCL thickness theoretically.	Simplified assumptions (*e.g.*, ideal interfaces); requires accurate input parameters.	Theoretical validation and predictive design of buffer layers/coatings.

related resistance and stabilizing interfacial reactions.[103] Despite the diversity of coating chemistries, their mechanistic influence converges on interfacial band modulation. *Operando* HAXPES studies by Hikima *et al.* directly revealed dynamic band bending at the Li_2MnO_3/LASGTP interface during charge–discharge processes.[33] Upon charging to 5.0 V, the interfacial electronic structure evolved from a staggered (Type-II) configuration to a flat-band (Type-I) alignment. Such transitions underscore that coatings—particularly buffer layers—effectively adjust the interfacial Fermi level alignment and mitigate potential discontinuities that drive space charge accumulation. During discharge, partial reduction at the interface further highlights the sensitivity of band structures to interfacial environments. These insights reveal that the true function of coating layers lies in the tailored engineering of interfacial band alignment, rather than merely preventing side reactions. Coatings regulate interfacial electrostatics, lower the interfacial potential drop, and reduce the driving force for Li^+ depletion or accumulation within the SCL. Consequently, coatings can be analyzed and compared through a unified descriptor—their capability to flatten or smooth the interfacial band landscape. Furthermore, this framework suggests a pathway for next-generation design: by rationally stacking coating layers with complementary band alignment characteristics, one may construct multi-step energy level transitions that impede electron leakage while enabling rapid Li^+ transport. Such engineered, asymmetric band structures may surpass single-layer coatings and offer a more robust route for suppressing SCL effects.[124,137–141]

5.1.2 Element doping as bulk-level band modulators. While surface coatings primarily regulate the interfacial band alignment, element doping functions as the second tier of Hierarchical Band Alignment Engineering, modulating the electronic structure, defect chemistry, and ionic conduction pathways within the bulk and subsurface regions of the cathode. Unlike coatings—which operate through interfacial

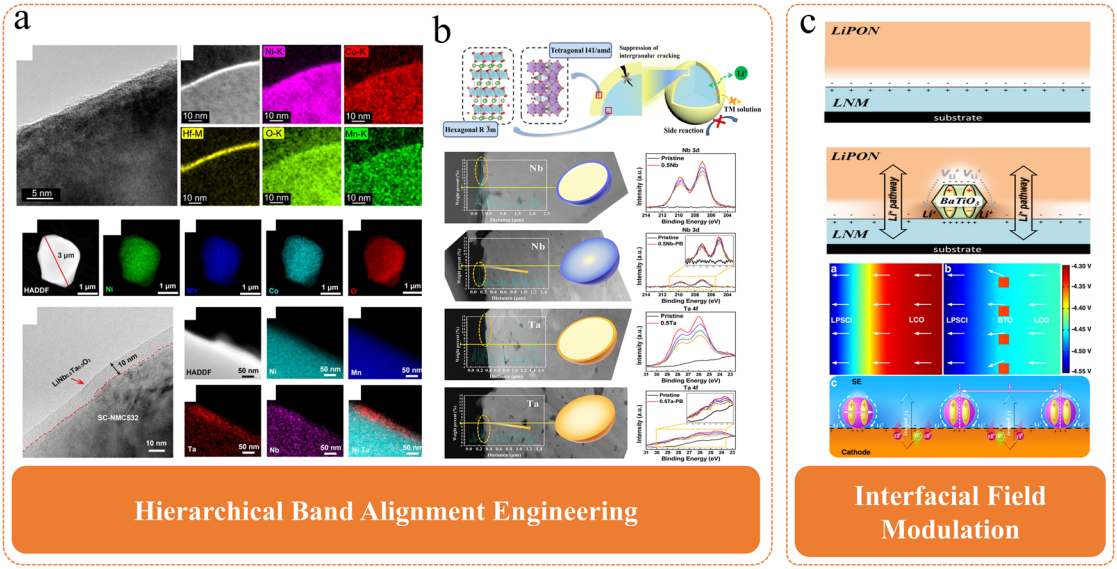

Fig. 12 Currently used methods to improve the space charge layer effect: (a) Coating. Reproduced with permission.[24] Copyright 2021, American Chemical Society. Reproduced with permission.[123] Copyright 2021, John Wiley and Sons, (b) Element doping. Reproduced with permission.[124] Copyright 2020, American Chemical Society. Reproduced with permission.[125] Copyright 2021, American Chemical Society, (c) Coating dielectric materials. Reproduced under terms of the CC-BY license.[50] Copyright 2020, Longlong Wang *et al.*, published by Springer Nature. Reproduced with permission.[69] Copyright 2014, John Wiley and Sons.

energy-level smoothing—doping indirectly reshapes the SCL by tuning the internal electrochemical potential distribution that governs Li^+ flux toward the interface. Doping introduces aliovalent ions into the transition-metal layers or lithium layers, thereby modifying the defect concentrations, altering the local lattice polarizability, and adjusting the bulk Fermi level position. These modifications shift the intrinsic band edges of the cathode and regulate the electrochemical potential gradient at the electrode–electrolyte interface. Consequently, doping can reduce the steepness of the interfacial potential drop, suppress excessive Li^+ depletion or accumulation, and weaken SCL-driven impedance growth.

Gradient doping further enhances these effects, as the spatial variation in dopant concentration yields a graded internal potential landscape. This gradual band alignment enables a smoother Li^+ diffusion transition from the bulk to the interface, effectively diminishing the formation intensity of the SCL. Lim *et al.*[21] demonstrated this principle by incorporating Ta and W through precursor surface modification on $LiNi_{0.6}Co_{0.2}Mn_{0.2}O_2$, creating a doped surface layer that stabilizes the cathode–sulfide electrolyte interface. Beyond single-ion doping, multi-element doping has emerged as a powerful strategy for simultaneously enhancing structural integrity and interfacial energetics. Lee *et al.*[125] introduced Al^{3+} and Nb^{5+} dual doping into $Li[Ni_{0.92}Co_{0.04}Mn_{0.04}]O_2$ (NCM92), achieving improved cycling stability by leveraging complementary mechanisms: Al_{3+} strengthened the host lattice, while Nb^{5+} refined primary particle morphology and modulated defect formation energies. This cooperative tuning of both structural stability and band energetics demonstrates the advantage of multicomponent doping in high-Ni cathodes.

Overall, element doping enriches the Hierarchical Band Alignment Engineering framework by offering bulk-level control over band structure, defect chemistry, and Li^+ chemical potential, all of which converge to weaken the space charge layer and enhance the electrochemical stability of all-solid-state Ni-rich cathodes. Notably, doping and coating can be synergistically combined to create multiscale band modulation. Liu *et al.* achieved this by pairing $La_2Li_{0.5}Al_{0.5}O_4$ coating with Al_{3+} doping on single-crystalline $LiNi_{0.8}Co_{0.1}Mn_{0.1}O_2$.[142] The dual modification reduced oxygen vacancy formation, suppressed internal cracking, and enhanced Li^+ transport kinetics. These findings highlight that doping and coating are not competing strategies; instead, they influence SCL formation from distinct but complementary dimensions. Coatings regulate interfacial band alignment directly, while doping tunes intrinsic bulk band structures and defect populations that feed into the interfacial electrochemical potential landscape.[31,33,77,143]

5.2 Interfacial field modulation

While Hierarchical Band Alignment Engineering focuses on smoothing electronic energy-level discontinuities, a complementary and equally important strategy is to directly regulate the built-in electric field that drives SCL formation at solid–solid interfaces. The intensity of this internal electric field originates from the electrochemical potential mismatch between the cathode and solid electrolyte; thus, mitigating band bending through electrostatic compensation offers a fundamentally different pathway to suppress SCL formation. Dielectric engineering introduces high-permittivity or ferroelectric materials at the interface to generate polarization

fields that counteract the intrinsic electric field. Wang *et al.*[50] demonstrated this concept by integrating discontinuous nano-ferroelectric domains at the cathode–electrolyte interface, showing that their switchable dipoles can partially neutralize the interfacial electrostatic field and significantly suppress SCL-driven impedance growth. Yada *et al.*[69] further confirmed the applicability of this approach using nano-ferrite domains, which enhanced cycling performance by mitigating polarization-induced Li^+ migration barriers. Building upon these findings, their group employed pulsed laser deposition to coat $LiCr_{0.05}Ni_{0.45}Mn_{1.5}O_{4-\delta}$ with discontinuous $BaTiO_3$ (BTO), achieving stable high-voltage cycling through effective suppression of band bending at the interface. In this framework, dielectric layers act as electric-field buffers and weaken the built-in potential responsible for SCL formation. Interfaces with high dielectric contrast can redistribute electric flux, attenuate the sharp potential drop, and weaken the electrostatic driving force for SCL formation. And the feasibility of this method has also been demonstrated in actual experiments. This makes the strategy particularly powerful when electronic bandgap engineering alone is insufficient—for example, when intrinsic band structures are difficult to manipulate without compromising cathode stability.

In summary, the strategies discussed above—Hierarchical Band Alignment Engineering and Interface Electric-Field Modulation—offer two powerful, complementary frameworks for suppressing the detrimental effects of the space charge layer. Band alignment engineering reconstructs the electronic landscape at the electrode–electrolyte interface through coatings and dopants, creating graded pathways that minimize potential discontinuities and homogenize Li^+ distribution. Dielectric and ferroelectric engineering, in contrast, directly compensates the built-in electric field that drives SCL formation, thereby weakening interfacial band bending and promoting smoother ion transport.[144–149] However, the effectiveness of both strategies fundamentally depends on the intrinsic chemical and mechanical stability of the interface. Artificially constructed layers—whether band-alignment coatings, doped surface regions, or dielectric modifiers—can only function as intended when the interface maintains structural coherence and chemical integrity during long-term cycling. If interfacial reactions, lattice distortion, microcracking, or delamination continuously occur, the engineered interlayers will lose contact, degrade, or undergo unintended reactions, leading to new potential gradients that re-initiate SCL formation. Therefore, chemical and mechanical stabilization provides the foundational prerequisite for all SCL-mitigation strategies. Only when the underlying interface remains stable over extended cycling can the deliberately designed interlayers reliably regulate band alignment and electric-field distribution.

6. Summary and prospects

Understanding and controlling the space charge layer at solid–solid interfaces is central to unlocking the full potential of ASSBs. In this review, we systematically examined the origin, evolution, and consequences of SCL formation through the integrated lenses of defect chemistry, interfacial band alignment, and electrostatic field redistribution. We further clarified how the SCL dynamically evolves during cycling, influencing ion migration kinetics, interfacial activation energy, electronic leakage pathways, and long-term chemo-mechanical integrity. Beyond consolidating existing knowledge, this review establishes a unified physical framework that categorizes SCL-regulation strategies into Hierarchical Band Alignment Engineering and Interfacial Electric-Field Modulation, highlighting the electrostatic essence of the SCL and offering a coherent roadmap for rational interface design (Fig. 13). However, despite significant progress, the complexity of the SCL at the interface of all-solid-state batteries is far from being fully elucidated. Future research should be committed to the following key directions to fundamentally overcome the constraints imposed by the SCL on the performance of all-solid-state batteries.

6.1 Multiphysics-coupled modeling of dynamic SCL evolution

Developing multi-physics, multi-scale theoretical frameworks is essential for describing the dynamic behavior of the SCL under realistic battery conditions. Existing models often oversimplify the strong coupling among electrochemical reactions, mechanical stress from volume changes, thermal gradients, and interfacial chemical evolution. High-fidelity, multi-scale computational approaches integrating density functional theory, molecular dynamics, phase-field modeling, and continuum electro-chemo-mechanics will be needed to accurately predict SCL evolution—its thickness, lithium-ion distribution, band bending, and internal fields—and to clarify its correlation with the structural evolution and oxygen release intrinsic to Ni-rich materials.

6.2 High-performance advanced characterization techniques for interfaces

Breakthroughs in *in situ*/quasi-*in situ* characterization with high spatial and temporal resolution are critical for validating theory and guiding interface design. Advanced techniques—such as DPC-STEM, EELS, HRTEM, HAXPES, synchrotron XAS, and multi-dimensional solid-state NMR—should be further developed to directly visualize Li^+ distribution, oxidation-state changes, lattice distortion, and local potential gradients within the SCL. Importantly, future tools must enable real-time observation of SCL evolution during charge–discharge cycling, thermal perturbation, and mechanical loading, allowing its effects to be decoupled from other interfacial processes and establishing causal links between electrostatic phenomena and performance degradation.

6.3 Interface design based on electronic-structure precision engineering

Interface design guided by band-structure engineering is expected to become a central strategy for SCL control.

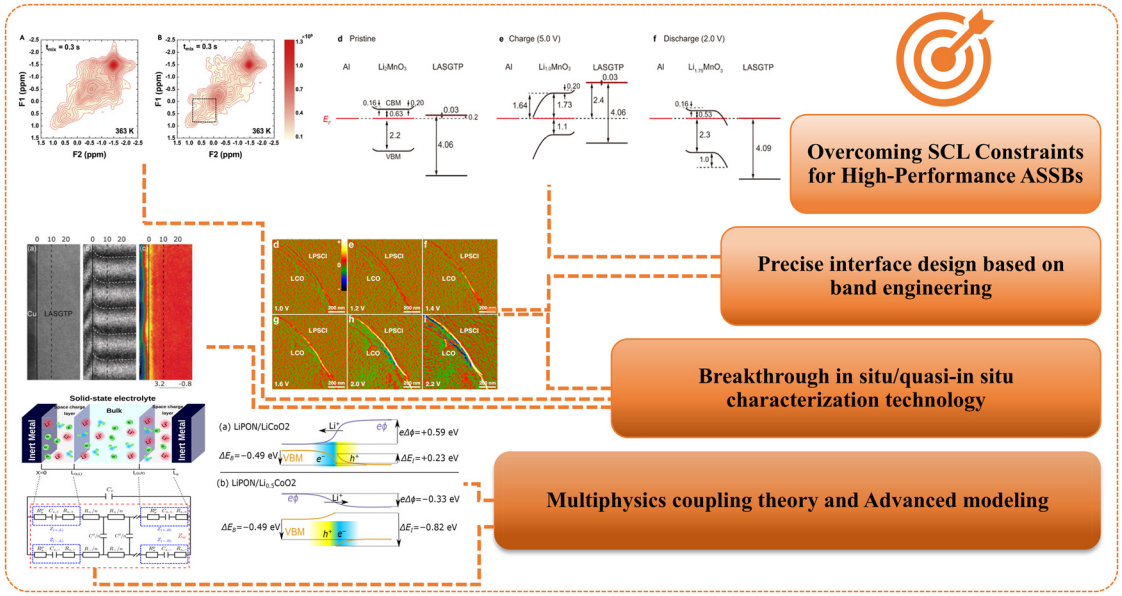

Fig. 13 Summary and outlook.

Conventional coatings, though effective, often rely on empirical optimization without a mechanistic foundation. Moving forward, functional interlayers with tailored electronic structures, graded band alignment, epitaxially engineered interfaces, and interface layers designed through high-throughput computational screening could enable precise Fermi level matching and controlled interfacial potential landscapes. Such strategies may not only suppress detrimental SCL formation but also create low-impedance Li^+ transport pathways and passivate reactive surfaces.

From a practical and industrial perspective, the two major SCL-regulation strategies discussed above—Hierarchical Band Alignment Engineering and Interfacial Electric-Field Modulation—exhibit distinct advantages, limitations, and applicable scenarios, depending on electrolyte chemistry, processing constraints, and scalability requirements. Hierarchical Band Alignment Engineering, encompassing surface coatings and bulk or gradient doping, is broadly applicable to both oxide- and sulfide-based solid electrolytes. Coating-based approaches are particularly effective for sulfide electrolytes, where large interfacial chemical potential mismatch and narrow Debye lengths give rise to intense local electric fields; in such systems, thin buffer layers can efficiently smooth band discontinuities and suppress excessive space charge accumulation. Bulk or gradient doping, in contrast, is more readily integrated into oxide-based cathode materials and benefits from mature synthesis protocols, offering relatively high scalability and compositional tunability at moderate cost. However, both coating and doping strategies require precise control over thickness, composition, and interfacial uniformity, and excessive processing complexity may limit their large-scale manufacturability.

Interfacial Electric-Field Modulation strategies, such as dielectric or ferroelectric engineering, provide a fundamentally different route by directly compensating the built-in electric field that drives SCL formation. These approaches are particularly attractive for systems in which intrinsic band alignment is difficult to optimize without compromising structural stability, such as high-voltage cathodes or interfaces with severe electronic mismatch. Nevertheless, the fabrication of high-quality dielectric or ferroelectric interlayers often relies on advanced deposition techniques and stringent thickness control, which may increase processing cost and pose challenges for large-area or high-throughput production. Moreover, their effectiveness is highly sensitive to interfacial mechanical integrity, as polarization-induced field compensation requires stable and continuous contact during long-term cycling.

Taken together, Hierarchical Band Alignment Engineering offers greater materials universality and scalability, while Interfacial Electric-Field Modulation provides stronger electrostatic regulation capability in electronically mismatched systems but with higher processing complexity. For practical implementation, these strategies should not be viewed as mutually exclusive; rather, their judicious combination—guided by electrolyte type, operating voltage window, and manufacturing constraints—will be essential for balancing performance gains, process complexity, and cost. Such a comparative, application-oriented understanding provides a rational basis for selecting SCL-regulation strategies in industrially relevant all-solid-state battery designs.

Finally, realizing SCL control at the full-cell level requires integrating these strategies within a multi-scale interface engineering framework. The SCL does not exist in isolation but is closely coupled with particle microstructure, electrode mesoscale packing, macroscopic stress distribution, and battery assembly conditions. Therefore, particle-level optimi-

zations (such as single-crystallization, controlled morphology, and densification) must be combined with mechanically adaptive solid electrolytes and rational stack-pressure designs to ensure robust, intimate contact that enables the engineered interfacial electrostatics to function reliably during long-term cycling. Importantly, although some studies argue that mechanical degradation dominates interfacial failure, this does not negate the role played by SCLs; rather, mechanical integrity is a prerequisite for SCL formation. Thus, SCL evolution and mechanical contact degradation are inherently coupled, and resolving both challenges will require integrated electro–chemo–mechanical strategies.

Conflicts of interest

The authors declare no conflict of interest.

Data availability

No new experimental datasets were generated in this review. All data supporting the analysis, figures, and discussions presented here are derived from previously published literature, as cited throughout the manuscript. Additional information, including processed data files, schematics, is available from the corresponding authors upon reasonable request.

Acknowledgements

This work was supported by the National Key R&D Program of China (2023YFB2503700).

References

1 M. Ahangari, B. Szalai, J. Lujan, M. Zhou and H. Luo, *Materials*, 2024, **17**, 801.
2 U. Kim, J. Park, A. Aishova, R. M. Ribas, R. S. Monteiro, K. J. Griffith, C. S. Yoon and Y. Sun, *Adv. Energy Mater.*, 2021, **11**, 2100884.
3 W. Yuan, W. Peng, C. Wu, N. Liu, C. Shen, Z. Xiao, J. Liu, C. Li, Y. Guo, Q. Huang, P. Zhang, H. Pan, L. Wen, L. Shi, L. Lu, D. Ren, K. Wu, M. Ouyang and X. Liu, *Adv. Energy Mater.*, 2025, **15**, 2405907.
4 Y. Wu, W. Zhang, X. Rui, D. Ren, C. Xu, X. Liu, X. Feng, Z. Ma, L. Lu and M. Ouyang, *Adv. Energy Mater.*, 2025, **15**, 2405183.
5 H. Pan, B. Zhao, H. Lai, Q. Huang, Z. Xiao, H. Liu, X. Chen, D. Ren, L. Lu, X. Liu and M. Ouyang, *Chem. Eng. J.*, 2025, **524**, 169639.
6 R. Li, Y. Mao, N. Chen, Q. Liu, J. Shao, Z. Liao, K. Qiu, P. Wang, S. Hao, X. Liao, H. Wang, Y. Wei, C. Guo, X. Liu, G. Zhu, D. Ren, L. Lu and M. Ouyang, *J. Energy Storage*, 2025, **106**, 114859.
7 W. Peng, J. Liu, W. Yuan, Q. Huang, P. Zhang, C. Li, Y. Guo, L. Wen, Z. Xiao, J. Liu, Y. Li, D. Ren, L. Lu, M. Ouyang and X. Liu, *ACS Appl. Mater. Interfaces*, 2025, **17**, 47112.
8 D. Kitsche, F. Strauss, Y. Tang, N. Bartnick, A. Kim, Y. Ma, C. Kübel, J. Janek and T. Brezesinski, *Batteries Supercaps*, 2022, **5**, e202100397.
9 X. Li, Q. Sun, Z. Wang, D. Song, H. Zhang, X. Shi, C. Li, L. Zhang and L. Zhu, *J. Power Sources*, 2020, **456**, 227997.
10 C. Doerrer, I. Capone, S. Narayanan, J. Liu, C. R. M. Grovenor, M. Pasta and P. S. Grant, *ACS Appl. Mater. Interfaces*, 2021, **13**, 37809.
11 J. Yang, X. Liang, H.-H. Ryu, C. S. Yoon and Y.-K. Sun, *Energy Storage Mater.*, 2023, **63**, 102969.
12 S. S. Zhang, *Energy Storage Mater.*, 2020, **24**, 247.
13 Q. Huang, J. Liu, X. Chen, P. Zhang, L. Lu, D. Ren, M. Ouyang and X. Liu, *Adv. Mater.*, 2025, **37**, 2410006.
14 S. Braun, C. Yada and A. Latz, *J. Phys. Chem. C*, 2015, **119**, 22281.
15 X. Kang, H. Lin, G. Xu, J. Tao, Y. Chen, K. Zhong, J.-M. Zhang and Z. Huang, *Phys. Rev. Mater.*, 2024, **8**, 105402.
16 L. Jia, J. Zhu, X. Zhang, B. Guo, Y. Du and X. Zhuang, *Electrochem. Energy Rev.*, 2024, **7**, 12.
17 R. R. Gaddam, L. Katzenmeier, X. Lamprecht and A. S. Bandarenka, *Phys. Chem. Chem. Phys.*, 2021, **23**, 12926.
18 Q. Zhang, Y. Kong, K. Gao, Y. Wen, Q. Zhang, H. Fang, C. Ma and Y. Du, *Sci. China: Technol. Sci.*, 2022, **65**, 2246.
19 Z. Xu, X. Wang, Z. Wang, X. Li, J. Liu, A. Bayaguud and L. Zhang, *J. Power Sources*, 2023, **571**, 233079.
20 J. Zhang, C. Zheng, L. Li, Y. Xia, H. Huang, Y. Gan, C. Liang, X. He, X. Tao and W. Zhang, *Adv. Energy Mater.*, 2020, **10**, 1903311.
21 C. B. Lim and Y. J. Park, *Sci. Rep.*, 2020, **10**, 10501.
22 H.-J. Noh, S. Youn, C. S. Yoon and Y.-K. Sun, *J. Power Sources*, 2013, **233**, 121.
23 R. Koerver, W. Zhang, L. De Biasi, S. Schweidler, A. O. Kondrakov, S. Kolling, T. Brezesinski, P. Hartmann, W. G. Zeier and J. Janek, *Energy Environ. Sci.*, 2018, **11**, 2142.
24 D. Kitsche, Y. Tang, Y. Ma, D. Goonetilleke, J. Sann, F. Walther, M. Bianchini, J. Janek and T. Brezesinski, *ACS Appl. Energy Mater.*, 2021, **4**, 7338.
25 D. H. Jeon, *Energy Storage Mater.*, 2019, **18**, 139.
26 H. Zhang, X. He, Z. Chen, Y. Yang, H. Xu, L. Wang and X. He, *Adv. Energy Mater.*, 2022, **12**, 2202022.
27 S.-T. Myung, F. Maglia, K.-J. Park, C. S. Yoon, P. Lamp, S.-J. Kim and Y.-K. Sun, *ACS Energy Lett.*, 2017, **2**, 196.
28 G. Xu, X. Liu, A. Daali, R. Amine, Z. Chen and K. Amine, *Adv. Funct. Mater.*, 2020, **30**, 2004748.
29 W. Schottky, *Z. Phys.*, 1942, **118**, 539.
30 K. Lehovec, *J. Chem. Phys.*, 1953, **21**, 1123.
31 J. Haruyama, K. Sodeyama, L. Han, K. Takada and Y. Tateyama, *Chem. Mater.*, 2014, **26**, 4248.

32 Z. Cheng, M. Liu, S. Ganapathy, C. Li, Z. Li, X. Zhang, P. He, H. Zhou and M. Wagemaker, *Joule*, 2020, **4**, 1311.
33 K. Hikima, K. Shimizu, H. Kiuchi, Y. Hinuma, K. Suzuki, M. Hirayama, E. Matsubara and R. Kanno, *Commun. Chem.*, 2022, **5**, 52.
34 S. Ohta, N. Singh, R. K. Rai, H. Koh, Y. Zhang, W. Suk, M. J. Palmer, S.-J. Hwang, M. Jones, C. Wang, C. Ling, K. S. Masias, E. Stavitski, J. Sakamoto and E. A. Stach, *Joule*, 2025, **9**, 101789.
35 N. J. J. De Klerk and M. Wagemaker, *ACS Appl. Energy Mater.*, 2018, **1**(10), 5609–5618.
36 F. Zhang, Y. Guo, L. Zhang, P. Jia, X. Liu, P. Qiu, H. Zhang and J. Huang, *eTransportation*, 2023, **15**, 100220.
37 J. Gao, J. Hao, Y. Gao, X. Sun, Y. Zhang, D. Song, Q. Zhao, F. Zhao, W. Si, K. Wang, T. Ohsaka, F. Matsumoto, J. Wu and H. Xie, *eTransportation*, 2023, **17**, 100252.
38 D. Ren, L. Lu, R. Hua, G. Zhu, X. Liu, Y. Mao, X. Rui, S. Wang, B. Zhao, H. Cui, M. Yang, H. Shen, C.-Z. Zhao, L. Wang, X. He, S. Liu, Y. Hou, T. Tan, P. Wang, Y. Nitta and M. Ouyang, *eTransportation*, 2023, **18**, 100272.
39 L. Wang, Z. Chen, Y. Liu, Y. Li, H. Zhang and X. He, *eTransportation*, 2023, **16**, 100239.
40 X. Yang, K. Doyle-Davis, X. Gao and X. Sun, *eTransportation*, 2022, **11**, 100152.
41 Z. Sun, M. Li, B. Xiao, X. Liu, H. Lin, B. Jiang, H. Liu, M. Li, D.-L. Peng and Q. Zhang, *eTransportation*, 2022, **14**, 100203.
42 A. Kim, S. Woo, M. Kang, H. Park and B. Kang, *Front. Chem.*, 2020, **8**, 468.
43 C. Loho, R. Djenadic, M. Bruns, O. Clemens and H. Hahn, *J. Electrochem. Soc.*, 2017, **164**, A6131.
44 A.-K. Hatz, R. Calaminus, J. Feijoo, F. Treber, J. Blahusch, T. Lenz, M. Reichel, K. Karaghiosoff, N. M. Vargas-Barbosa and B. V. Lotsch, *ACS Appl. Energy Mater.*, 2021, **4**, 9932.
45 M. V. Reddy, C. M. Julien, A. Mauger and K. Zaghib, *Nanomaterials*, 2020, **10**, 1606.
46 J. Janek and W. G. Zeier, *Nat. Energy*, 2016, **1**, 16141.
47 M. Fingerle, R. Buchheit, S. Sicolo, K. Albe and R. Hausbrand, *Chem. Mater.*, 2017, **29**, 7675.
48 K. Mizushima, P. C. Jones, P. J. Wiseman and J. B. Goodenough, *Mater. Res. Bull.*, 1980, **15**, 783.
49 Y. Nomura, K. Yamamoto, T. Hirayama, S. Ouchi, E. Igaki and K. Saitoh, *Angew. Chem.*, 2019, **131**, 5346.
50 L. Wang, R. Xie, B. Chen, X. Yu, J. Ma, C. Li, Z. Hu, X. Sun, C. Xu, S. Dong, T.-S. Chan, J. Luo, G. Cui and L. Chen, *Nat. Commun.*, 2020, **11**, 5889.
51 J. Maier, *J. Phys. Chem. Solids*, 1985, **46**, 309.
52 N. Togasaki, A. Nakao, T. Tanaka, U. Harada, H. Onish, H. Yasuda, S. Kobayashi, F. Maeda and T. Osaka, *J. Electrochem. Soc.*, 2023, **170**, 050519.
53 M. Haruta, S. Shiraki, T. Suzuki, A. Kumatani, T. Ohsawa, Y. Takagi, R. Shimizu and T. Hitosugi, *Nano Lett.*, 2015, **15**, 1498.
54 C. Yu, S. Ganapathy, E. R. H. Van Eck, L. Van Eijck, N. De Klerk, E. M. Kelder and M. Wagemaker, *J. Energy Chem.*, 2019, **38**, 1.
55 Z. Moradi, A. Lanjan, R. Tyagi and S. Srinivasan, *J. Energy Storage*, 2023, **73**, 109048.
56 P. Ranque, E. Gonzalo, M. Armand and D. Shanmukaraj, *Mater. Today Energy*, 2023, **34**, 101283.
57 H. Wang, J. Zhu, Y. Su, Z. Gong and Y. Yang, *Sci. China: Chem.*, 2021, **64**, 879.
58 C. König, A. Ramanayagam, J. Kraus and B. Roling, *Batteries Supercaps*, 2024, **7**, e202300578.
59 K. Yamamoto, Y. Iriyama, T. Asaka, T. Hirayama, H. Fujita, C. A. J. Fisher, K. Nonaka, Y. Sugita and Z. Ogumi, *Angew. Chem., Int. Ed.*, 2010, **49**, 4414.
60 C. Yu, S. Ganapathy, E. R. H. V. Eck, H. Wang, S. Basak, Z. Li and M. Wagemaker, *Nat. Commun.*, 2017, **8**, 1086.
61 K. Yamamoto, Y. Iriyama, T. Asaka, T. Hirayama, H. Fujita, C. A. J. Fisher, K. Nonaka, Y. Sugita and Z. Ogumi, *Angew. Chem.*, 2010, **122**, 4516.
62 Z. Gu, J. Ma, F. Zhu, T. Liu, K. Wang, C.-W. Nan, Z. Li and C. Ma, *Nat. Commun.*, 2023, **14**, 1632.
63 D. Brogioli, F. Langer, R. Kun and F. La Mantia, *ACS Appl. Mater. Interfaces*, 2019, **11**, 11999.
64 L. Katzenmeier, S. Helmer, S. Braxmeier, E. Knobbe and A. S. Bandarenka, *ACS Appl. Mater. Interfaces*, 2021, **13**, 5853.
65 L. Katzenmeier, L. Carstensen and A. S. Bandarenka, *ACS Appl. Mater. Interfaces*, 2022, **14**, 15811.
66 P. Lu, S. Gong, C. Wang, Z. Yu, Y. Huang, T. Ma, J. Lian, Z. Jiang, L. Chen, H. Li and F. Wu, *ACS Nano*, 2024, **18**, 7334.
67 R. Koerver, I. Aygün, T. Leichtweiß, C. Dietrich, W. Zhang, J. O. Binder, P. Hartmann, W. G. Zeier and J. Janek, *Chem. Mater.*, 2017, **29**, 5574.
68 Y. Tateyama, B. Gao, R. Jalem and J. Haruyama, *Curr. Opin. Electrochem.*, 2019, **17**, 149.
69 C. Yada, A. Ohmori, K. Ide, H. Yamasaki, T. Kato, T. Saito, F. Sagane and Y. Iriyama, *Adv. Energy Mater.*, 2014, **4**, 1301416.
70 C. Zhu, S. Kobayashi, Y. Sugisawa, F. Weber, K.-H. Lin, M. Kitamura, K. Horiba, H. Kumigashira, K. Nishio, R. Shimizu, D. Sekiba, T. Hitosugi and R. Berger, *ACS Nano*, 2025, **19**, 39062.
71 Y.-F. Zhou, M.-Z. Yang, F.-Q. She, L. Gong, X.-Q. Zhang, J. Chen, S.-Q. Song and F.-Y. Xie, Application of X-ray photoelectron spectroscopy to study interfaces for solid-state lithium ion battery, *Acta Phys. Sin.*, 2021, **70**, 178801.
72 B. Wang, M. S. R. Limon, Y. Zhou, K. Cho, Z. Ahmad and L. Su, *ACS Energy Lett.*, 2025, **10**, 1255.
73 T. Kim, K. Kim, S. Lee, G. Song, M. S. Jung and K. T. Lee, *Chem. Mater.*, 2022, **34**, 9159.
74 A. Neumann, S. Randau, K. Becker-Steinberger, T. Danner, S. Hein, Z. Ning, J. Marrow, F. H. Richter, J. Janek and A. Latz, *ACS Appl. Mater. Interfaces*, 2020, **12**, 9277.
75 S. Huang, Y. Kimura, T. Nakamura, N. Ishiguro, O. Sekizawa, K. Nitta, T. Uruga, T. Takeuchi, T. Okumura, M. Tada, Y. Uchimoto and K. Amezawa, *J. Phys. Chem. C*, 2024, **128**, 6213.

76 Y. Zhang, Y. Tian, Y. Xiao, L. J. Miara, Y. Aihara, T. Tsujimura, T. Shi, M. C. Scott and G. Ceder, *Adv. Energy Mater.*, 2020, **10**, 1903778.
77 Y. Chen, L. Huang, D. Zhou, X. Gao, T. Hu, Z. Zhang, Z. Zhen, X. Chen, L. Cui and G. Wang, *Adv. Energy Mater.*, 2024, **14**, 2304443.
78 Y. Han, S. H. Jung, H. Kwak, S. Jun, H. H. Kwak, J. H. Lee, S. Hong and Y. S. Jung, *Adv. Energy Mater.*, 2021, **11**, 2100126.
79 Y. Liu, Y. Bai, W. Jaegermann, R. Hausbrand and B.-X. Xu, *ACS Appl. Mater. Interfaces*, 2021, **13**, 5895.
80 W. He, L. Zhou, M. K. Tufail, P. Zhai, P. Yu, R. Chen and W. Yang, *Trans. Tianjin Univ.*, 2021, **27**, 423.
81 L. Katzenmeier, M. Gößwein, A. Gagliardi and A. S. Bandarenka, *J. Phys. Chem. C*, 2022, **126**, 10900.
82 R. Usiskin and J. Maier, *Adv. Energy Mater.*, 2021, **11**, 2001455.
83 M. S. Whittingham, *Chem. Rev.*, 2004, **104**, 4271.
84 Y. Wang, T. Liu, L. Estevez and J. Kumar, *Energy Storage Mater.*, 2020, **27**, 232.
85 S. Sinzig, T. Hollweck, C. P. Schmidt and W. A. Wall, *J. Electrochem. Soc.*, 2023, **170**, 040513.
86 W.-L. Feng, F. Wang, X. Zhou, X. Ji, F.-D. Han and C.-S. Wang, Stability of interphase between solid state electrolyte and electrode, *Acta Phys. Sin.*, 2020, **69**, 228206, DOI: 10.7498/aps.69.20201554.
87 M. W. Swift and Y. Qi, *Phys. Rev. Lett.*, 2019, **122**, 167701.
88 W. Jiang, Q. Zhou, F. Lu, Y. Chen and Z. Ma, *J. Energy Storage*, 2022, **55**, 105655.
89 M. W. Swift, H. Jagad, J. Park, Y. Qie, Y. Wu and Y. Qi, *Curr. Opin. Solid State Mater. Sci.*, 2022, **26**, 100990.
90 A. Al-Ali, B. Maundy, A. Allagui and A. Elwakil, *J. Electroanal. Chem.*, 2022, **924**, 116854.
91 K. Nishio, D. Imazeki, K. Kurushima, Y. Takeda, K. Edamura, R. Nakayama, R. Shimizu and T. Hitosugi, *ACS Appl. Mater. Interfaces*, 2022, **14**, 34620.
92 S. Jayasubramaniyan, C. Lee and H.-W. Lee, *J. Mater. Res.*, 2022, **37**, 4017.
93 D. Wang, X. Yin, J. Wu, Y. Luo and S. Shi, *Acta Phys.-Chim. Sin.*, 2024, **40**, 2307029.
94 S. Su, J. Ma, L. Zhao, K. Lin, Q. Li, S. Lv, F. Kang and Y. He, *Carbon Energy*, 2021, **3**, 866.
95 Y. Huang, B. Shao and F. Han, *Curr. Opin. Electrochem.*, 2022, **33**, 100933.
96 A. Chakraborty, M. Dixit, D. Aurbach and D. T. Major, *npj Comput. Mater.*, 2018, **4**, 60.
97 B.-Y. Chang, *Electrochim. Acta*, 2023, **462**, 142741.
98 J. Sugiyama, E. Nocerino, O. K. Forslund, Y. Sassa, M. Månsson, S. Kobayashi, K. Nishio, T. Hitosugi, A. Suter and T. Prokscha, *J. Phys.: Conf. Ser.*, 2023, **2462**, 012046.
99 J. A. Isaac, L. R. Mangani, D. Devaux and R. Bouchet, *ACS Appl. Mater. Interfaces*, 2022, **14**, 13158.
100 H. Masuda, N. Ishida, Y. Ogata, D. Ito and D. Fujita, *Nanoscale*, 2017, **9**, 893.
101 N. C. Paranamana, A. Werbrouck, A. K. Datta, X. He and M. J. Young, *Adv. Energy Mater.*, 2024, 2403904.
102 M. Liu, S. Ganapathy and M. Wagemaker, *Acc. Chem. Res.*, 2022, **55**, 333.
103 M. Liu, C. Wang, C. Zhao, E. Van Der Maas, K. Lin, V. A. Arszelewska, B. Li, S. Ganapathy and M. Wagemaker, *Nat. Commun.*, 2021, **12**, 5943.
104 Z. Feng, X. Qiu, X. Chen, H. Wang and X. Guo, *ACS Appl. Mater. Interfaces*, 2024, **16**, 42995.
105 T. Zhang, Z. Yang, H. Li, Q. Zhuang and Y. Cui, *Acta Chim. Sin.*, 2019, **77**, 525.
106 T. Hakari, M. Deguchi, K. Mitsuhara, T. Ohta, K. Saito, Y. Orikasa, Y. Uchimoto, Y. Kowada, A. Hayashi and M. Tatsumisago, *Chem. Mater.*, 2017, **29**, 4768.
107 Y.-H. Chen, S.-C. Lin, J.-A. Wang, S.-Y. Hsu and C.-C. M. Ma, *J. Electrochem. Soc.*, 2018, **165**, A3029.
108 B. Fan, Z. Guan, H. Wang, L. Wu, W. Li, S. Zhang and B. Xue, *Solid State Ionics*, 2021, **368**, 115680.
109 H. Li, T. Zhang, Z. Yang, Y. Shi, Q. Zhuang and Y. Cui, *Int. J. Electrochem. Sci.*, 2021, **16**, 210229.
110 C. Wei, H. Xue, Z. Li, F. Zhao and F. Tang, *J. Phys. D: Appl. Phys.*, 2022, **55**, 105305.
111 C.-Y. Yu, J. Choi, J. Dunham, R. Ghahremani, K. Liu, P. Lindemann, Z. Garver, D. Barchiesi, R. Farahati and J.-H. Kim, *J. Power Sources*, 2024, **597**, 234116.
112 Z. Tang, A. Morchhale, J. R. Sayre and J.-H. Kim, *J. Energy Storage*, 2025, **107**, 114966.
113 R. Götz, M. Wagner, K. Song, L. Katzenmeier and A. S. Bandarenka, *Batteries Supercaps*, 2024, e202400570.
114 Q. Huang, K. Qiu, Z. Xiao, D. Li, H. Deng, L. Wen, W. Yuan, W. Peng, P. Zhang, J. Liu, D. Li, C. Zhan, X. Chen, L. Lu, J. Hua, Y. Wei, J. Shao, D. Ren, M. Ouyang and X. Liu, *Adv. Funct. Mater.*, 2025, **35**, 2422663.
115 Q. Huang, H. Pan, D. Wang, Z. Xiao, Y. Guo, S. Liu, J. Liu, G. Yuan, T. Cheng, L. Wen, C. Li, Y. Li, J. Liu, Y. Wei, X. Rui, J. Hua, X. Chen, J. Shao, D. Ren, B. Deng, S. Yin, L. Lu, X. Liu and M. Ouyang, *Adv. Funct. Mater.*, 2025, e16819.
116 P. Zhang, J. Liu, Q. Huang, Y. Li, Y. Guo, Z. Xiao, C. Li, L. Wen, W. Peng, W. Yuan, G. Zhu, L. Yin, L. Fan, L. Zheng, J. Zhang, T. Tan, J. Hua, D. Ren, L. Lu and X. Liu, *eTransportation*, 2025, **26**, 100493.
117 J. Liu, C. Wang, J. Yu, Q. Huang, P. Zhang, Z. Xiao, S. Liu, W. Yuan, C. Li, W. Peng, X. Yan, Y. Zhang, L. Yin, M. Zhang, L. Zheng, J. Zhang, J. Xu, W. Yin, L. Lu, D. Ren, M. Ouyang and X. Liu, *Nano Energy*, 2025, **140**, 111038.
118 W. Jiang, X. Zhu, R. Huang, S. Zhao, X. Fan, M. Ling, C. Liang and L. Wang, *Adv. Energy Mater.*, 2022, **12**, 2103473.
119 A. Masias, J. Marcicki and W. A. Paxton, *ACS Energy Lett.*, 2021, **6**, 621.
120 M. Jiang, D. L. Danilov, R. Eichel and P. H. L. Notten, *Adv. Energy Mater.*, 2021, **11**, 2103005.
121 S. H. Jung, U. Kim, J. Kim, S. Jun, C. S. Yoon, Y. S. Jung and Y. Sun, *Adv. Energy Mater.*, 2020, **10**, 1903360.
122 X. Liu, B. Zheng, J. Zhao, W. Zhao, Z. Liang, Y. Su, C. Xie, K. Zhou, Y. Xiang, J. Zhu, H. Wang, G. Zhong, Z. Gong, J. Huang and Y. Yang, *Adv. Energy Mater.*, 2021, **11**, 2003583.

123 C. Wang, S. Hwang, M. Jiang, J. Liang, Y. Sun, K. Adair, M. Zheng, S. Mukherjee, X. Li, R. Li, H. Huang, S. Zhao, L. Zhang, S. Lu, J. Wang, C. V. Singh, D. Su and X. Sun, *Adv. Energy Mater.*, 2021, **11**, 2100210.
124 Y. Huang, S. Cao, X. Xie, C. Wu, S. Jamil, Q. Zhao, B. Chang, Y. Wang and X. Wang, *ACS Appl. Mater. Interfaces*, 2020, **12**, 19483.
125 J. S. Lee and Y. J. Park, *ACS Appl. Mater. Interfaces*, 2021, **13**, 38333.
126 U. Nisar, N. Muralidharan, R. Essehli, R. Amin and I. Belharouak, *Energy Storage Mater.*, 2021, **38**, 309.
127 S. Kang, H. Kim, J. Y. Jung, K.-H. Park, K. Kim, J. H. Song, J.-S. Yu, Y.-J. Kim and W. Cho, *ACS Appl. Mater. Interfaces*, 2023, **15**, 10744.
128 F. Walther, S. Randau, Y. Schneider, J. Sann, M. Rohnke, F. H. Richter, W. G. Zeier and J. Janek, *Chem. Mater.*, 2020, **32**, 6123.
129 S. Payandeh, D. Goonetilleke, M. Bianchini, J. Janek and T. Brezesinski, *Curr. Opin. Electrochem.*, 2022, **31**, 100877.
130 K. Jung and T. Yim, *Rare Met.*, 2021, **40**, 2793.
131 M. Akin, Y. Wang, X. Qiao, Z. Yan and X. Zhou, *Electrochim. Acta*, 2020, **355**, 136779.
132 S. Payandeh, C. Njel, A. Mazilkin, J. H. Teo, Y. Ma, R. Zhang, A. Kondrakov, M. Bianchini and T. Brezesinski, *Adv. Mater. Interfaces*, 2023, **10**, 2201806.
133 Y. Wang, E. Wang, X. Zhang and H. Yu, *Energy Fuels*, 2021, **35**, 1918.
134 C. Wang, Y. Wu, S. Wang, E. Van Der Heide and X. Zhuang, *Mater. Res. Bull.*, 2025, **181**, 113078.
135 R. Ruess, S. Schweidler, H. Hemmelmann, G. Conforto, A. Bielefeld, D. A. Weber, J. Sann, M. T. Elm and J. Janek, *J. Electrochem. Soc.*, 2020, **167**, 100532.
136 N. Ohta, K. Takada, I. Sakaguchi, L. Zhang, R. Ma, K. Fukuda, M. Osada and T. Sasaki, *Electrochem. Commun.*, 2007, **9**, 1486.
137 R. Götz, E. Pugacheva, Z. Ahaliabadeh, P. S. Llanos, T. Kallio and A. S. Bandarenka, *ChemSusChem*, 2024, **17**, e202401026.
138 X. Li, L. Jin, D. Song, H. Zhang, X. Shi, Z. Wang, L. Zhang and L. Zhu, *J. Energy Chem.*, 2020, **40**, 39.
139 B. Shen, L. Li, X. Yao and B. Huang, *Ceram. Int.*, 2024, **50**, 7150.
140 R. Zhang, Y. Ma, Y. Tang, D. Goonetilleke, T. Diemant, J. Janek, A. Kondrakov and T. Brezesinski, *Chem. Mater.*, 2023, **35**, 6835.
141 Y. Zou, K. Zhou, G. Liu, N. Xu, X. Zhang, Y. Yang, J. Zhang and J. Zheng, *ACS Appl. Mater. Interfaces*, 2021, **13**, 16427.
142 Y. Liu, T. Zeng, G. Li, T. Wan, M. Li, X. Zhang, M. Li, M. Su, A. Dou, W. Zeng, Y. Zhou, R. Guo and D. Chu, *Energy Storage Mater.*, 2022, **52**, 534.
143 K. Yang, Y. Sun, Q. Su, Y. Lu, K. Liu, Z. Li, H. Liu and L. Zhang, *Chem. Eng. J.*, 2023, **471**, 144405.
144 W. Liu, P. Oh, X. Liu, M. Lee, W. Cho, S. Chae, Y. Kim and J. Cho, *Angew. Chem., Int. Ed.*, 2015, **54**, 4440.
145 M. Liu, S. Zhang, E. R. H. Van Eck, C. Wang, S. Ganapathy and M. Wagemaker, *Nat. Nanotechnol.*, 2022, **17**, 959.
146 W. Li, M. Li, S. Wang, P.-H. Chien, J. Luo, J. Fu, X. Lin, G. King, R. Feng, J. Wang, J. Zhou, R. Li, J. Liu, Y. Mo, T.-K. Sham and X. Sun, *Nat. Nanotechnol.*, 2025, **20**, 265.
147 S. Deng, X. Li, Z. Ren, W. Li, J. Luo, J. Liang, J. Liang, M. N. Banis, M. Li, Y. Zhao, X. Li, C. Wang, Y. Sun, Q. Sun, R. Li, Y. Hu, H. Huang, L. Zhang, S. Lu, J. Luo and X. Sun, *Energy Storage Mater.*, 2020, **27**, 117.
148 J. Liang, S. Hwang, S. Li, J. Luo, Y. Sun, Y. Zhao, Q. Sun, W. Li, M. Li, M. N. Banis, X. Li, R. Li, L. Zhang, S. Zhao, S. Lu, H. Huang, D. Su and X. Sun, *Nano Energy*, 2020, **78**, 105107.
149 T.-T. Zuo, R. Rueß, R. Pan, F. Walther, M. Rohnke, S. Hori, R. Kanno, D. Schröder and J. Janek, *Nat. Commun.*, 2021, **12**, 6669.